Studying the interaction between charm and light-flavor mesons

S. Acharya *et al.*[*]

(ALICE Collaboration)

The two-particle momentum correlation functions between charm mesons ($D^{*\pm}$ and $D^{\pm}$) and charged light-flavor mesons ($\pi^{\pm}$ and $K^{\pm}$) in all charge combinations are measured for the first time by the ALICE Collaboration in high-multiplicity proton–proton collisions at a center-of-mass energy of $\sqrt{s} = 13$ TeV. For DK and D^*K pairs, the experimental results are in agreement with theoretical predictions of the residual strong interaction based on quantum chromodynamics calculations on the lattice and chiral effective field theory. In the case of $D\pi$ and $D^*\pi$ pairs, tension between the calculations including strong interactions and the measurement is observed. For all particle pairs, the data can be adequately described by Coulomb interaction only, indicating a shallow interaction between charm and light-flavor mesons. Finally, the scattering lengths governing the residual strong interaction of the $D\pi$ and $D^*\pi$ systems are determined by fitting the experimental correlation functions with a model that employs a Gaussian potential. The extracted values are small and compatible with zero.

I. INTRODUCTION

The exploration of the strong interaction within hadrons remains a pivotal question in particle physics. Quantum chromodynamics (QCD) has been well tested at distances significantly shorter than the nucleon's size, and many high-energy phenomena can be effectively explained through perturbative QCD at the quark level. However, when the distance between quarks reaches the nucleon size, the QCD becomes a strongly coupled theory and the low-energy processes between hadrons are not yet well described. From the experimental point of view, the residual strong interaction between hadrons has been studied in the past using scattering experiments at low energies with both stable and unstable beams. Numerous results have been achieved for nucleon–nucleon interactions with this method [1,2], however, due to the experimental challenge in realizing scattering experiments with unstable particles, only a reduced set of measurements could have been performed in the strange sector and none in the charm sector. In order to overcome these experimental limitations, the femtoscopy technique has emerged as an interesting tool to study reactions among hadrons [3]. This method is based on the measurement of the correlation function of pairs of hadrons in momentum space, which

encodes the information of the interaction between the two hadrons convoluted with the emitting source distribution. The ALICE Collaboration measured the residual strong interaction between several light and strange hadrons using the femtoscopy technique in high-multiplicity proton–proton (pp) collisions, including pp, $pK^{\pm}$, $p\Lambda$, $p\bar{\Lambda}$, $p\Sigma^0$, $\Lambda\Lambda$, $\Lambda\bar{\Lambda}$, $p\Xi^-$, $p\Omega^-$, $p\phi$, and ΛK interactions [4–14].

The study of hadronic interactions involving charm mesons (D, D^*) has gained significant interest after the observation of the charm-strange meson $D_{s0}^*(2317)$ [15–17], whose mass lies significantly below the quark model [18] predictions ($m_{\text{experiment}} - m_{\text{quark model}} \approx 100$ MeV/c^2), preventing its accommodation in simple constituent quark models [19]. The puzzle of the $D_{s0}^*(2317)$ low mass has led to a range of theories, such as those based on the concepts of conventional charm-strange mesons with coupled-channel impacts [20–26], or of $D^{(*)}K$ molecule [27–31], or of a tetraquark state composed of $c q \bar{s} \bar{q}$ (anti)quarks [32–34]. Models based on a mixture of tetraquark and molecular states were also proposed [35,36]. In recent years, several exotic hadrons with charm-quark content have been discovered, such as the $\chi_c 1(3872)$ [37], T_{cc}^+ [38,39], $P_c(4312)$, $P_c(4440)$, and $P_c(4457)$ [21,40,41] states. Similarly to the $D_{s0}^*(2317)$, these states can be interpreted as $D\bar{D}^*$, DD^*, or $\Sigma_c\bar{D}$, $\Sigma_c\bar{D}^*$ molecular states, or compact multiquark states [42–45]. The observation of potential molecular states is, however, not the only measurement that challenges the charm-hadron spectrum in terms of the conventional quark model. In fact, the masses of the nonstrange $D_0^*(2300)$ and $D_1(2430)$ charm mesons [46–48] are very similar to the corresponding states in the charm-strange spectrum, $D_{s0}^*(2317)$ and $D_{s1}(2460)$ [15,17,21], while they are expected to be smaller. When

---

[*]Full author list given at the end of the article.

combining chiral effective field theory with quantum chromodynamics calculations on the lattice, all low-energy open heavy-flavor mesonic states with positive parity can be classified as hadronic molecules. In this framework, pions, kaons, and η mesons arise as Goldstone bosons and, by computing the $D\pi$, $D\eta$, and $D_s\bar{K}$ coupled-channel scatterings, a bound state with a large coupling to the $D\pi$ channel is obtained at a mass that corresponds to the $D_0^*(2300)$ state [49–53]. Nevertheless, their structures remain uncertain owing to the lack of direct experimental information on the residual strong interaction between charm and light hadrons. These measurements are particularly challenging because conventional scattering experiments with charm hadrons are restricted by their short lifetime. Only recently, the residual strong final state interaction involving charm hadrons became experimentally accessible thanks to the femtoscopy technique. The first study of the strong interaction between charm mesons and nucleons (pD^-) was published by the ALICE Collaboration in Ref. [54], proving the feasibility of applying the femtoscopy technique to the charm sector.

The knowledge of interactions between charm particles and light-flavor hadrons is also essential for the study of ultrarelativistic heavy-ion collisions. In these collisions, a color-deconfined state of matter, called quark-gluon plasma (QGP), is formed [55–59]. Due to the early production, charm quarks are recognized as ideal probes of the QGP, and measurements of the yields and angular anisotropies of charm hadrons can be used to infer information about the QGP properties [60,61]. However, during the hadronic phase following the deconfined state of the system, the charm hadrons can interact with the other particles produced in the collision, which are mainly light-flavor hadrons, via elastic and inelastic processes. These interactions modify the momentum and angular distributions of heavy-flavor hadrons in heavy-ion collisions. Therefore, the scattering parameters of the charm hadrons with light-flavor hadrons, in particular, pions and kaons, must be determined to disentangle this effect from those related to the QGP formation [62].

In this article, the first measurement of the residual strong interaction between nonstrange charm and light-flavor mesons via the femtoscopy technique is presented. This method relies on the fact that particles with similar momentum, hence small relative momentum, can interact with each other strongly, if they are emitted at small relative distance. The momentum correlation functions of the charm mesons D^+ and D^{*+} with charged pions and kaons, also simply referred to as light-flavor mesons in the following, are measured for all charge combinations in pp collisions at $\sqrt{s} = 13$ TeV. Section II contains the description of the experimental apparatus, the selection of charm and light-flavor mesons, as well as the single-particle properties (e.g., purity), which are later needed to extract the final results from the raw experimental data.

The measurement of the correlation functions is described in Sec. III, while the evaluation of the systematic uncertainties is discussed in Sec. IV. Finally, the results are presented and compared to model calculations in Sec. V.

II. EVENT AND PARTICLE SELECTION

This analysis is performed on a data sample of pp collisions at $\sqrt{s} = 13$ TeV collected with the ALICE [13] experiment during the LHC Run 2 data-taking period. The events are selected employing a high-multiplicity (HM) trigger. The multiplicity is estimated using the V0 detector, which consists of an array of scintillators located at forward ($2.8 < \eta < 5.1$) and backward ($-3.7 < \eta < -1.7$) pseudorapidity [63]. The multiplicity estimator is the V0 amplitude, which is related to the energy deposited by ionizing particles in the V0 detector. The triggered events correspond to the 0–0.17% percentile of the inelastic events with the highest V0 amplitude and with at least one charged track in the range $|\eta| < 1$ (INEL > 0). The resulting HM dataset consists of approximately 1.0×10^9 inelastic pp collisions with, on average, 30 charged particles per event in the pseudorapidity interval $|\eta| < 0.5$ [10]. Charged-particle tracks are reconstructed using both the inner tracking system (ITS) [64] and the time projection chamber (TPC) [65], which are embedded in a uniform magnetic field of 0.5 T along the beam direction. They cover the full azimuthal angle and the pseudorapidity interval $|\eta| < 0.9$. The position of the primary vertex is obtained from the reconstructed tracks, and the particle identification (PID) is performed employing both the TPC and the time-of-flight (TOF) [66] detectors.

The PYTHIA 8.243 event generator [67] is used in the Monte Carlo (MC) simulations. The generated particles are transported through a simulation of the ALICE apparatus using Geant 3 [68]. Events and tracks are reconstructed employing the same algorithms as used for real collision data [69], and a selection on large charged-particle multiplicities is applied to mimic the effect of the HM trigger.

A. Light-meson selection

The K^+ and π^+ candidates are identified using PID information provided by the TPC and TOF, via the specific energy loss dE/dx and time-of-flight, respectively. For each track, the deviation of the measured quantity with respect to the expected value for a particular particle-species hypothesis in terms of units of the detector resolution is computed and denoted as $n_\sigma^{\mathrm{TPC/TOF}}$. Pion candidates with transverse momentum $p_{\mathrm{T}} < 0.5$ GeV/c are identified using only the TPC dE/dx signal via a selection of $|n_\sigma^{\mathrm{TPC}}(\pi)| < 3$. For larger p_{T} the PID information of TPC and TOF is combined into $n_\sigma^{\mathrm{comb}} = \sqrt{(n_\sigma^{\mathrm{TPC}})^2 + (n_\sigma^{\mathrm{TOF}})^2}$ and a selection of $n_\sigma^{\mathrm{comb}} < 3$ is applied. Tracks with $p_{\mathrm{T}} > 0.5$ GeV/c which do not have a TOF signal are discarded. The PID selection of the kaon candidates is performed similarly with an

additional more complex set of selections on n_σ^{TPC} and n_σ^{comb}, not only for kaons but also for electrons and pions, in order to suppress possible contamination to the kaon sample in specific momentum regions [14].

The pion and kaon candidates are selected in the p_{T} ranges [0.14, 4.0] and [0.15, 2.15] GeV/c, respectively. The lower limit is imposed to suppress the light-meson candidates stemming from interactions with the detector material. The tracks are required to be reconstructed from more than 80 clusters in the TPC to assure a good quality of the track, good p_{T} resolution at large momenta, as well as to remove fake tracks from the sample. In addition, the candidates are selected within a pseudorapidity range of $|\eta| < 0.8$. To suppress the contribution of particles coming from weak decays or interactions with the detector material, a selection on the distance of closest approach (DCA) to the primary vertex in the transverse plane xy and along the beam axis direction z is applied. For kaons, $\mathrm{DCA}_{xy}^{\mathrm{K}} < 0.1$ cm and $\mathrm{DCA}_z^{\mathrm{K}} < 0.2$ cm are required, while for pions $\mathrm{DCA}_{xy,z}^{\pi} < 0.3$ cm.

The purity of the pion and kaon samples, defined as the ratio of the correctly identified particles over the total number of candidates, is computed as a function of p_{T} using MC simulations and is reweighted by the p_{T} distribution of the pion or kaon candidates that form a pair with $\mathrm{D}^{(*)+}$ mesons at low relative momentum. It is found to be 99% for pions and 98% for kaons.

The particles can be classified according to their origin: the ones that do not come from interactions with the material of the detector are classified as primary or secondary, according to the ALICE definition [70]. The fraction of each contribution is estimated with a template fit to the DCA distribution. The templates for the DCA distributions of primary particles, secondaries from weak decays, and secondaries from interactions in the material are obtained from MC simulations. The primary fractions are found to be 99.5% and 99.8% for pions and kaons, respectively. A portion of identified primary light-flavor mesons comes, however, from the strong decay of long-lived resonances ($c\tau > 5$ fm). As the fractions of this contribution cannot be determined via DCA template fits, they are estimated with the ThermalFist statistical hadronization model [71]. The resonances that contribute the most to the pion yield are the η and ω mesons, while in the case of kaons it is the ϕ meson. The resulting primary fractions of pions and kaons, subtracted of the contribution of such long-lived resonances, are found to be about 88% and 94%, respectively. These values are used in the following analysis as primary fractions.

B. Charm-meson selection

The D^+, D^{*+}, and D^0 candidates are reconstructed via the hadronic decay channels $\mathrm{D}^+ \to \mathrm{K}^-\pi^+\pi^+$, $\mathrm{D}^{*+} \to \mathrm{D}^0\pi^+$, followed by $\mathrm{D}^0 \to \mathrm{K}^-\pi^+$, and their charge conjugates. The branching ratios (BR) of the considered D^+, D^{*+}, and D^0 decays are BR = $(9.38 \pm 0.16)\%$, BR = $(67.7 \pm 0.5)\%$, and BR = $(3.947 \pm 0.030)\%$, respectively [72]. The tracks fulfilling a set of standard quality selections [54] are combined with the correct charge signs to build D^+- and D^{*+}-meson candidates. The obtained sample of charm-meson candidates consists of three different classes: candidates that result from the combination of uncorrelated pions and kaons form the *combinatorial background*, charm mesons that come from the hadronization of a charm quark or the decay of excited open-charm or charmonium states, which are referred to as *prompt*, and $\mathrm{D}^{(*)+}$ mesons that come from the decay of beauty hadrons, which are referred to as *nonprompt*.

To separate the prompt, nonprompt, and combinatorial background contributions, the decay-vertex topology, in combination with the PID information is used. The mean proper decay length of $\mathrm{D}^\pm$ and D^0 mesons is about 312 μm and 123 μm, respectively, while for beauty hadrons it is close to 500 μm [72]. Topological variables, such as the DCA of the charm meson candidate, the D^+ (D^0) decay length, and the cosine of the pointing angle, namely the angle between the D^+ (D^0) momentum and the line that passes through the primary and secondary vertices, are exploited by a multiclass machine learning (ML) algorithm based on boosted decision trees (BDT). The ML model, provided by the XGBoost library [73,74], is trained using labeled examples of candidates of each class. The samples of prompt and nonprompt D^+ and D^{*+} mesons are obtained from a PYTHIA 8 simulation with enhanced production of heavy-flavor hadrons, where only events that contain a $c\bar{c}$ or $b\bar{b}$ pair are selected, and the charm mesons are forced to decay in the hadronic decay channels of interest for the analysis. The background sample for D^+ is obtained from the data by selecting the sidebands of the candidate invariant-mass distribution. For D^{*+} mesons, the right sideband of the invariant-mass difference $\Delta M = M(\mathrm{K}\pi\pi) - M(\mathrm{K}\pi)$ is used. To prepare the sample for the training, loose selections on the PID and decay-vertex topology are applied. The training is performed in several p_{T} intervals. Then, the model is applied to the data, assigning scores to each candidate, which are related to the probabilities that the candidate belongs to each of the three classes. To suppress the combinatorial background and enhance the prompt contribution in the sample, candidates with a low background-score and high prompt-score are selected; the selections are chosen such that they maximize the expected significance and purity.

The fraction of nonprompt candidates present in the sample is estimated with a data-driven procedure that relies on the fact that the prompt selection efficiencies change differently to the nonprompt ones when the selection on the ML scores is changed. For each selection i on the ML scores, the raw yield Y_i of charm-meson candidates is extracted via a fit to the invariant-mass distribution of the

charm-meson candidates. The fit function is the sum of a Gaussian, for the description of the signal, and an exponential or an exponential multiplied by a power law for the description of the background in the case of D^+ and D^{*+} mesons, respectively. The left panel of Fig. 1 shows an example of fit to the ΔM distribution of D^{*+} candidates with $2.2 < p_T < 2.4$ GeV/c. The raw yield is related to the corrected yields of prompt (N_{prompt}) and nonprompt ($N_{nonprompt}$) mesons via

$$\delta_i = Y_i - (\mathrm{Acc} \times \epsilon)_{\mathrm{prompt},i} \times N_{\mathrm{prompt}}$$
$$- (\mathrm{Acc} \times \epsilon)_{\mathrm{nonprompt},i} \times N_{\mathrm{nonprompt}}, \qquad (1)$$

where $(\mathrm{Acc} \times \epsilon)_{\mathrm{prompt/nonprompt}}$ is the product of acceptance and efficiency for each selection, and δ_i are the residuals that account for the equation not holding exactly because of the uncertainties. The definition of multiple sets of selections leads to an overdetermined system of equations, out of which the corrected yields can be extracted via a χ^2 minimization. Further details are provided in Ref. [75]. An example of a raw-yield distribution as a function of the BDT-based selection used in the minimization procedure for D^{*+} mesons with $2.2 < p_T < 2.4$ GeV/c is shown in the right panel of Fig. 1. The leftmost data point of the distribution represents the raw yield corresponding to the loosest selection on the BDT output related to the candidate probability of being a nonprompt D^{*+} meson, while the rightmost one corresponds to the strictest selection, which is expected to preferentially select nonprompt D^{*+} mesons. The prompt and nonprompt components obtained from the minimization procedure are represented by the red and blue filled histograms, respectively. The nonprompt fraction extracted in p_T intervals is reweighted with the p_T distribution of the $D^{(*)+}$ mesons that form pairs at low k^*. The extracted nonprompt fractions are $(7.2 \pm 0.2)\%$ for $D\pi$ and DK, and $(7.7 \pm 1.3)\%$ for $D^*\pi$ and D^*K.

The prompt component of the D^+-meson sample also includes mesons that come from the decay of excited charm states. The main contribution comes from the decay of the D^{*+} mesons, via the $D^{*\pm} \to D^{\pm} + \pi^0$ and $D^{*\pm} \to D^{\pm} + \gamma$ decays, that have a branching ratio of $(30.7 \pm 0.5)\%$ and $(1.6 \pm 0.4)\%$, respectively [72]. Since the strong final-state interaction (FSI) is only accessible via the study of the primary particles, the D^+ mesons that result from the decay of charm resonances represent a source of background. Unlike the contribution of D^+ mesons from beauty-hadron decays, it is not possible to experimentally separate it with the procedure described above, due to the short lifetime of the D^{*+} resonances ($c\tau \approx 2400$ fm) [72]. The fraction of D^+ mesons originating from D^{*+} decays is estimated in Ref. [54], employing the production cross sections of D^+ and D^{*+} mesons in pp collisions at $\sqrt{s} = 5.02$ TeV [75,76] and a simulation with PYTHIA 8.2 for the description of the $D^{*\pm} \to D^{\pm} + X$ decay kinematics. It is estimated to be $(27.6 \pm 1.3(\mathrm{stat}) \pm 2.4(\mathrm{syst}))\%$.

To obtain a high-purity sample of $D^{(*)+}$-meson candidates, the following procedure is used. The distribution of the invariant mass of the D^+-meson candidates and invariant-mass difference of the D^{*+}-meson candidates is fitted in several p_T intervals, from 1 to 10 GeV/c.
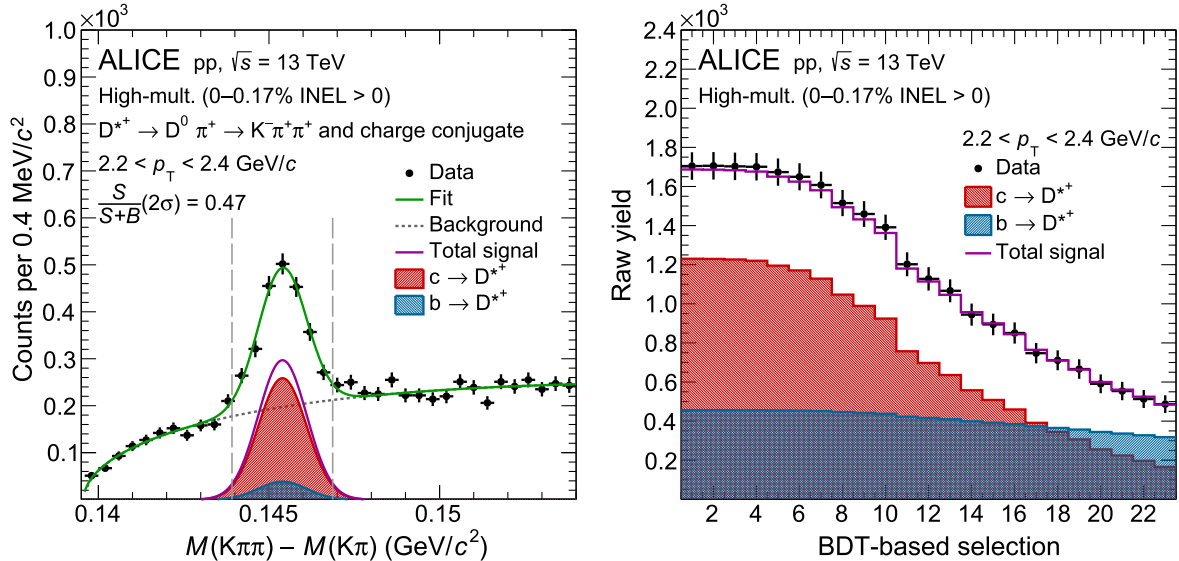

FIG. 1. Left: distribution of invariant-mass difference for D^{*+} candidates in the $2.2 < p_T < 2.4$ GeV/c interval. The green solid line shows the total fit function and the gray dotted line the combinatorial background. The contributions of D^{*+} mesons originating from charm hadronization and beauty-hadron decays are obtained with the method relying on the definition of different selection criteria, as explained in the text. Right: example of raw-yield distribution as a function of the BDT-based selection for the $2.2 < p_T < 2.4$ GeV/c interval, employed in the procedure adopted for the determination of the fraction of D^{*+} originating from beauty-hadron decays.

The sample of $D^{(*)+}$ mesons used for the analysis is obtained by applying a selection to the invariant mass of the candidates, which is defined by a 2σ window around the nominal mass, $M_{D^\pm} = 1869.66 \pm 0.05$ MeV/c^2 and $M_{D^{*\pm}} = 2010.26 \pm 0.05$ MeV/c^2 [72], where σ is the width of the fitted Gaussian. This selection range is represented by the vertical dashed lines in Fig. 1. The purity is computed as the ratio of the signal candidates over the total number of candidates in this invariant-mass range, where the number of signal candidates is extracted with a fit to the invariant-mass distribution. This results in a p_T-integrated purity of around 71% for D^+ mesons and 67% for D^{*+} mesons.

III. THE CORRELATION FUNCTION

In this analysis, the interaction between the charm mesons $D^{(*)}$ and the light-flavor mesons π and K is investigated employing the correlation function [77], defined as

$$C(k^*) = \mathcal{N} \times \frac{N_{\text{same}}(k^*)}{N_{\text{mixed}}(k^*)}, \tag{2}$$

where $k^* = \frac{1}{2} \times |\boldsymbol{p}_1^* - \boldsymbol{p}_2^*|$ is the relative momentum of two particles with momentum $\boldsymbol{p}_1$ and $\boldsymbol{p}_2$ in the pair rest frame, denoted by the asterisk, $\mathcal{N}$ is a normalization constant, and $N_{\text{same (mixed)}}(k^*)$ is the k^* distribution of the pairs measured in the same (mixed) events. The mixed-event distribution, which does not contain any effect of the strong FSI, reflects the phase space of the underlying event. Therefore, it serves as a reference to which the same-event distribution can be compared in order to extract information on the strong FSI of a specific system. To ensure a good quality of the reference sample, N_{mixed}, the mixing is performed only between events with similar multiplicity and primary-vertex position [5,7,10]. As the same (mixed) event distributions of the pairs are found to be compatible with the ones of the respective charge conjugates, they are combined

in order to enhance the statistical precision. In the following, same-charge $D^{(*)}X$ refers to $D^{(*)+}X^+ \oplus D^{(*)-}X^-$ pairs, while opposite-charge $D^{(*)}X$ refers to $D^{(*)+}X^- \oplus D^{(*)-}X^+$ pairs, where X is either K or π. The normalization constant $\mathcal{N}$ is chosen such that the mean value of the correlation function equals unity in a given range at large k^*, where the particles are not close enough in momentum space to experience FSI. The number of pairs and the normalization range for the different channels are reported in Table I. The latter are chosen according to the shape of the same (mixed) event distributions, which decreases and flattens out at different k^* regions depending on the involved light-flavor meson. The experimental correlation functions are computed in k^* intervals of 50 MeV/c, and the horizontal position of each data point is the average of the k^* distribution of the mixed event in the corresponding k^* interval. The effect of the finite momentum resolution of the ALICE detector on data is found to be negligible.

The experimental correlation functions involving D^+ and light-flavor mesons, obtained from Eq. (2), are shown in the left panels of Figs. 2 and 3. They are raw quantities, which can be decomposed as

$$C_{\text{raw}}(k^*) = C_{\text{femto}}(k^*) \times C_{\text{nonfemto}}(k^*), \tag{3}$$

where $C_{\text{femto}}(k^*) = \sum_{i,j} \lambda_{i,j} \times C_{i,j}(k^*)$, with $C_{i,j}(k^*)$ arising from the FSI between the ith and jth components of the two particle species involved in the analysis, namely primary, secondary, and misidentified particles. Each of these contributions is weighted according to so-called λ parameters, which are computed as $\lambda_{ij} = p_i p_j f_i f_j$ where $p_{i,j}$ and $f_{i,j}$ are, respectively, the purities and primary (secondary) fractions of the ith and jth contributions to the particle samples, discussed in Sec. II A. The contribution to $C_{\text{femto}}(k^*)$, that only includes primary signal particles, is also referred to as genuine correlation function $C_{\text{gen}}(k^*)$ and is used to extract the relevant physics information about the strong FSI for the pair of interest. A detailed discussion

TABLE I. Number of pairs with small relative momenta, where final-state effects become relevant and in the full k^* range, as well as the normalization range for the individual particle pair combinations under investigation.

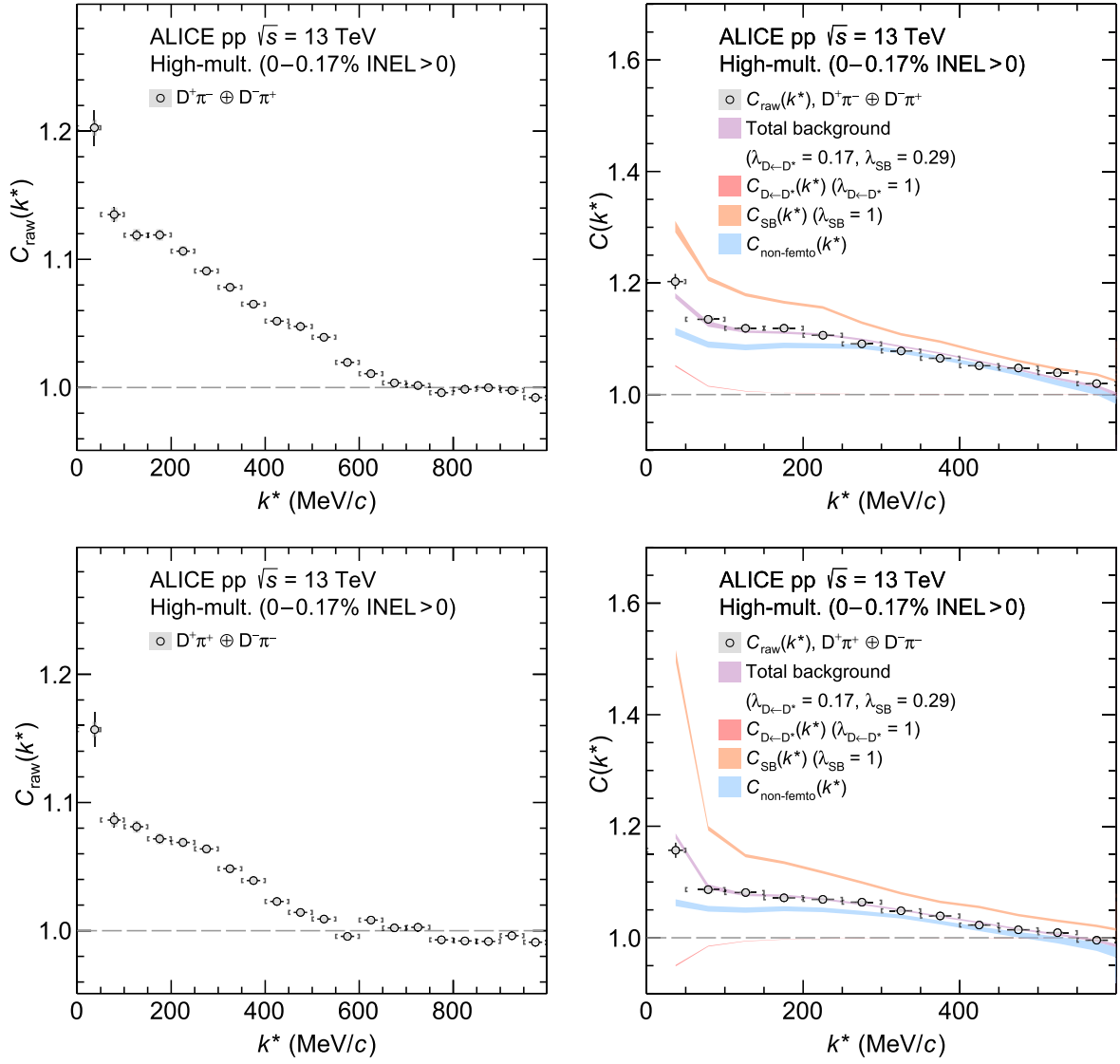|	Number of pairs in $N_{\text{same}}(k^*)$		
Pair	Total	$k^* < 200$ MeV/c	Normalization range
$D^+\pi^+ \oplus D^-\pi^-$	3.0×10^6	2.0×10^5	$k^* \in [1.0, 1.5]$ GeV/c
$D^+\pi^- \oplus D^-\pi^+$	2.9×10^6	2.1×10^5	
$D^+K^+ \oplus D^-K^-$	1.7×10^5	1.9×10^3	$k^* \in [1.5, 2.0]$ GeV/c
$D^+K^- \oplus D^-K^+$	1.6×10^5	2.2×10^3	
$D^{*+}\pi^+ \oplus D^{*-}\pi^-$	4.7×10^5	3.3×10^4	$k^* \in [1.5, 2.0]$ GeV/c
$D^{*+}\pi^- \oplus D^{*-}\pi^+$	4.8×10^5	3.4×10^4	
$D^{*+}K^+ \oplus D^{*-}K^-$	4.9×10^4	479	$k^* \in [1.5, 2.0]$ GeV/c
$D^{*+}K^- \oplus D^{*+}K^-$	4.8×10^4	477	

FIG. 2.   Experimental $D\pi$ raw correlation functions $[C_{\mathrm{raw}}(k^*)]$ with statistical (bars) and systematic uncertainties (boxes) (left column) and background contributions to the experimental correlation functions (right column). The width of the bands corresponds to the total uncertainty $\sigma_{\mathrm{tot}} = \sqrt{\sigma_{\mathrm{stat}}^2 + \sigma_{\mathrm{syst}}^2}$. The violet band describes the total background, fitted to the data, and used to extract the genuine correlation function from the raw signal. This band consists of several contributions, which are also shown individually in the figure, scaled by the appropriate λ parameter. The results are shown for opposite-charge (first row) and same-charge (second row) pairs.

on the different contributions to $C_{\mathrm{femto}}(k^*)$ can be found in Sec. III A. The remaining residual backgrounds, not related to FSI, are included in the term $C_{\mathrm{nonfemto}}(k^*)$, which is discussed in Sec. III B.

A. Contributions related to FSI

There are several contributions to $C_{\mathrm{femto}}(k^*)$ in Eq. (3) in the case of $D^{(*)+}$ and light-flavor mesons. When it is not possible to constrain them experimentally, these contributions can be modeled using the Koonin-Pratt equation [77],

$$C(k^*) = \int \mathrm{d}^3 r^* S(r^*) |\psi(r^*, k^*)|^2, \qquad (4)$$

where the so-called source function $S(r^*)$ contains the distribution of the relative distance in the pair rest frame, and $\psi(r^*, k^*)$ denotes the two-particle wave function, which contains the interaction. Together they determine the shape of the correlation function, which is sensitive to the strong FSI at small $k^* < 200$ MeV/c, also denoted as femtoscopic region.

The source is constrained from the core-resonance model [78], which is based on the hypothesis of a common
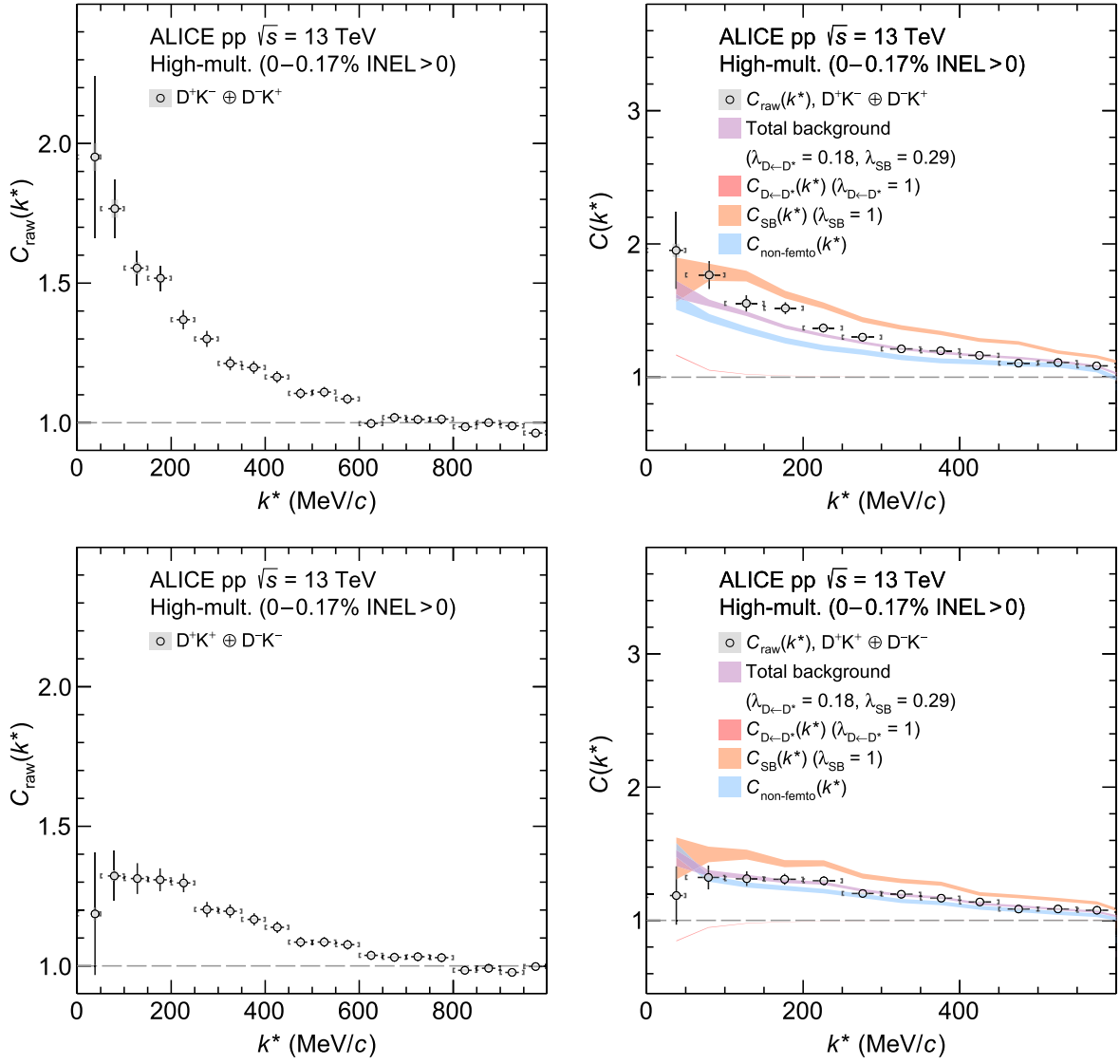
FIG. 3. Experimental DK raw correlation functions $[C_{\mathrm{raw}}(k^*)]$ with statistical (bars) and systematic uncertainties (boxes) (left column) and background contributions to the experimental correlation functions (right column). The width of the bands corresponds to the total uncertainty $\sigma_{\mathrm{tot}} = \sqrt{\sigma_{\mathrm{stat}}^2 + \sigma_{\mathrm{syst}}^2}$. The violet band describes the total background, fitted to the data, and used to extract the genuine correlation function from the raw signal. This band consists of several contributions, which are also shown individually in the figure, scaled by the appropriate λ parameter. The results are shown for opposite-charge (first row) and same-charge (second row) pairs.

emission source of all hadrons [79] and is anchored to $p - p$ correlation data in pp collisions. The model is characterized by a m_{T}-dependent Gaussian core of width r_{core}, from which all primordial particles, which are created directly during the hadronization process, and do not stem from an intermediate decay, are emitted. Therefore, by measuring the m_{T} of the reconstructed particle pairs with small k^* it is possible to obtain the respective core radius from a parametrization of the p–p data used in the model, following several previous femtoscopic analyses [6,7,10–12,54,80]. The mean m_{T} of $\mathrm{D}^{(*)}\pi$ pairs with $k^* < 200$ MeV/c is about 2.55 GeV/c^2, while it is approximately 2.66 GeV/c^2 for $\mathrm{D}^{(*)}$K pairs. This leads to core

radii of $r_{\mathrm{core}}^{\mathrm{D}^{(*)}\pi} = 0.82_{-0.07}^{+0.07}$ fm and $r_{\mathrm{core}}^{\mathrm{D}^{(*)}\mathrm{K}} = 0.81_{-0.07}^{+0.08}$ fm for $\mathrm{D}^{(*)}\pi$ and $\mathrm{D}^{(*)}$K pairs, respectively. However, also short-lived resonances feeding into the yields of the particles of interest have to be considered, as they lead to an effective enlargement of the source. This is accounted for in the core-resonance model by fixing the yields of the resonances and employing an event generator to model their propagation and relative spatial orientation. At large r^* these resonances lead to an exponential tail in the Gaussian-shaped source distributions obtained from the model for both $\mathrm{D}^{(*)}$K and $\mathrm{D}^{(*)}\pi$. Therefore, the effective source employed in this analysis is obtained by parametrizing the distributions with two Gaussian sources of width r_{eff}^i, which are combined

TABLE II. Parameters of the effective source $S_{\text{eff}}(r^*)$, which is given by the weighted sum of two Gaussian distributions of width r_{eff}^i and used in the modeling of the correlation functions. The difference between the $D^{(*)}\pi$ and $D^{(*)}K$ systems is due to the different transverse mass of the systems as well as resonances feeding into the light-flavor mesons.

Pair	w	r_{eff}^1 [fm]	r_{eff}^2 [fm]
$D^{(*)}K$	$0.78^{+0.02}_{-0.01}$	$0.86^{+0.09}_{-0.07}$	$2.03^{+0.19}_{-0.12}$
$D^{(*)}\pi$	$0.66^{+0.03}_{-0.02}$	$0.97^{+0.09}_{-0.08}$	$2.52^{+0.36}_{-0.20}$

with the weight w, leading to $S_{\text{eff}}(r^*) = wS_1(r^*) + (1-w)S_2(r^*)$. The values of the source parameters can be found in Table II. Employing $S_{\text{eff}}(r^*)$ as source function in Eq. (4) ultimately leads to two properly weighted correlation functions with the respective Gaussian sources, $S_1(r^*)$ and $S_2(r^*)$. The two-particle wave function $\psi(\mathbf{r}^*, \mathbf{k}^*)$ can be obtained by numerically solving the Schrödinger equation for a given interaction potential, for example by employing CATS [81], a correlation analysis tool using the Schrödinger equation.

The relevant contribution to $C_{\text{femto}}(k^*)$, needed to extract information of the strong FSI between $D^{(*)}\pi$ and $D^{(*)}K$, is the genuine correlation function $C_{\text{gen}}(k^*)$, which is associated to primary light-flavor mesons and signal $D^{(*)+}$ candidates.

As the $D^{(*)+}$-meson samples are not pure, the correlation between combinatorial background candidates and light-flavor mesons has to be taken into account, which arises from the interaction between the light-flavor mesons and the particles from which the background $D^{(*)+}$-meson candidate is built from [82]. It is estimated using a data-driven approach, where pions or kaons are paired with a pure sample of background $D^{(*)+}$ mesons, obtained from the sidebands of the invariant-mass intervals outside the $D^{(*)+}$-meson signal region. The resulting correlation function is referred to as $C_{\text{SB}}(k^*)$.

For the D^+ mesons, the sideband intervals start at $5\,\sigma_D$ away from the nominal mass and extend for 200 MeV/c^2. The σ_D corresponds to the width of the Gaussian function describing the signal peak and is determined via a fit to the invariant-mass distribution, considering its p_T dependence. For the D^{*+} mesons, the selection is analogous except that, instead of the invariant mass, the invariant-mass difference $M(K\pi\pi) - M(K\pi)$ is used, and only the right sideband is considered.

Since a contamination from D^{*+}-meson is expected in the D^+-meson sideband sample, due to $D^{*+} \to D^0\pi^+$ and subsequent $D^0 \to K^-\pi^+$ decays, the invariant-mass interval $[1.992, 2.028]$ MeV/c^2 is excluded. This corresponds to $2.5\sigma_{D^*}$ around the D^{*+} mass. The correlation functions obtained from the left and right sidebands are compatible within the uncertainties and combined as a weighted average, considering the relative abundances of background

in the left and right half of the D^+-meson signal region. The correction of the combinatorial $D^*\pi$ correlation function requires a different approach with respect to the traditional sideband method. This is due to the presence of an additional source of correlated background that arises from the correlation of a soft pion of a real D^{*+} decay with a background D^{*+} candidate formed by the D^0 meson coming from the same D^{*+} decay of the soft pion and an unrelated pion. Such a correlation results in a peak in the correlation function at $k^* \approx 40$ MeV/c, which cannot be removed via pair- or particle-level selections since the particle's origin is not known in data. For this reason, the correction for the combinatorial background cannot be carried out via a sideband analysis. Instead, the background-corrected correlation function is directly computed as

$$C'_{\text{raw}}(k^*) = \mathcal{N} \frac{p_{\text{same}}(k^*)N_{\text{same}}(k^*)}{p_{\text{mixed}}(k^*)N_{\text{mixed}}(k^*)}, \qquad (5)$$

where $p_{\text{same/mixed}}(k^*)$ is the purity of the D^{*+}-meson sample, calculated in the same- and mixed-events, as a function of k^*. Since the peak in the correlation function comes from the combinatorial background of the D^{*+}-meson candidates, a reweighting by the purity removes by construction the artifact at $k^* \approx 40$ MeV/c. The opposite-charge D^*K correlation function is affected by a similar issue since the D^0 meson decays into K^- via $D^0 \to K^-\pi^+$. However, in this case, the peak associated with the correlated background is found to be at $k^* \approx 600$ MeV/c, outside the femtoscopic region. As the correlation function above 200 MeV/c does not carry information about the strong FSI, the traditional sideband method is used to correct for the combinatorial background.

As already discussed in Sec. II B, a significant fraction of the D^+ mesons is produced from the decays of charm-hadron resonances. As this contribution cannot be separated experimentally, it is modeled using the Koonin-Pratt formalism with Coulomb potential, which is found to adequately describe the experimental correlation functions involving D^{*+} mesons, presented in Sec. V. Subsequently, the so obtained correlation functions are mapped into the ones of $(D^+ \leftarrow D^{*+})\pi$ and $(D^+ \leftarrow D^{*+})K$ pairs, respectively. The transformation of the momentum basis is performed using GENBOD phase-space simulations [83] of the $D^{*\pm} \to D^{\pm}\pi^0$ decay, as in this case the kinematics are most stringently constrained. Contributions to the D^+-meson yield from decays of other excited charm resonances are considered to be negligible [72].

A flat correlation function is assumed for sources of background that are not expected to lead to correlations, or that can be assumed negligible due to their small λ scaling parameter. They include contributions from particle pairs involving nonprimary light-flavor mesons and contamination of the samples, as well as nonprompt $D^{(*)+}$ mesons. Especially, the correlation of primary light-flavor mesons

with nonprompt D^+ mesons is studied in analogy to D^+ mesons from D^* decays, assuming Coulomb-only interaction, as it is associated to a non-negligible λ parameter of $\sim 5\%$. The decay kinematics for $B^+ \to D^+ + X$ decay is simulated, and the correlation function of B mesons and light-flavor meson pairs is mapped into one of the daughter D^+ and light-flavor mesons. As the phase space available for the decay is much larger compared to the $D^{*+} \to D^+$ case, the information on the interaction between beauty and light-flavor hadrons is lost, leading to a flat correlation.

In total, four(three) contributions to $C_{\text{femto}}(k^*)$ of the $D^{(*)}K$ and $D^{(*)}\pi$ systems can be identified. The individual λ_{ij} parameters are combined, based on how the corresponding correlation functions are obtained: λ_{gen} is associated with the correlation function obtained from primary signal particles only, λ_{SB} to the one from $D^{(*)+}$-meson background candidates, $\lambda_{D \leftarrow D^*}$ to the one obtained using D^+ mesons from D^{*+}-meson decays, and λ_{flat} contains all other femtoscopic contributions. The combined λ parameters for each system can be found in Table III.

B. Residual contributions

Energy-momentum conservation effects and the production of particles within jetlike structures introduce an enhancement of the correlation function and represent a residual background $C_{\text{nonfemto}}(k^*)$ not related to FSI and already introduced in Eq. (3), which has to be taken into account. The contribution of jetlike structures was observed in several meson–meson [4,84–87], meson–baryon [5,11], and baryon–antibaryon [12] femtoscopic analyses. They are related to initial hard processes at the parton level [88] and not to femtoscopic FSI. The correlation function used to model the residual background, $C_{\text{nonfemto}}(k^*)$, is obtained from MC simulations, where the FSI is absent. It is further multiplied by a constant N, which is a free parameter and accounts for a possible bias due to the chosen normalization region of the raw data. In the case of the $D\pi$ and D^*K systems, an additional polynomial of the form $p(k^*) = ak^{*2}$ and $p(k^*) = ak^*$, respectively, are added to the MC correlation function $C_{\text{MC}}(k^*)$ to better fit the background model to $C_{\text{raw}}(k^*)$ at intermediate k^*. This introduces an additional free parameter a and leads to the following expression for the residual background $C_{\text{nonfemto}}(k^*) = N \times [C_{\text{MC}}(k^*) + p(k^*)]$.

TABLE III. List of λ parameters, which quantify the individual contributions to the different raw correlation functions investigated in this paper.

	$D\pi$	DK	$D^*\pi$	$D^{*+}K^+ \oplus D^{*-}K^-$	$D^{*+}K^- \oplus D^{*+}K^-$
λ_{gen}	0.40	0.43	0.80	0.55	0.59
λ_{SB}	0.29	0.29	–	0.32	0.28
λ_{flat}	0.14	0.10	0.20	0.13	0.13
$\lambda_{D_{D \leftarrow D^*}}$	0.17	0.18	–	–	–

C. Modeling of the correlation function

In order to extract the unknown $C_{\text{gen}}(k^*)$ from the raw data, which is needed to study the residual strong interaction between the different particle pairs of interest, a model is built according to Eq. (3), taking into account all the relevant background contributions discussed in the previous sections.

In the case of $D\pi$ and DK pairs, all the sources of background, mentioned and explained in detail in Secs. III A and III B, are present. Therefore, the model takes the form

$$C_{\text{raw}}(k^*) = \lambda_{\text{SB}} C_{\text{SB}}(k^*) + C_{\text{nonfemto}}(k^*)[\lambda_{\text{gen}} C_{\text{gen}}(k^*) + \lambda_{D \leftarrow D^*} C_{D \leftarrow D^*}(k^*) + \lambda_{\text{flat}}], \quad (6)$$

where $C_{\text{SB}}(k^*)$ is the correlation function arising from the D^+-meson combinatorial background, $C_{\text{nonfemto}}(k^*)$ is the correlation function that describes the residual correlation not associated to FSI and mainly coming from jetlike contributions, and $C_D \leftarrow D^*(k^*)$ is the correlation function associated to the D^+ mesons from D^{*+} decays. Finally, λ_{flat} accounts for all femtoscopic background contributions, assumed to be flat. Notably, as $C_{\text{SB}}(k^*)$ is obtained in a data-driven approach, it already includes possible residual jetlike contributions and thus does not have to be multiplied by $C_{\text{nonfemto}}(k^*)$.

The model for the D^*K correlation functions is similar to the one used for $D\pi$ and DK correlations, with the difference that the contribution from excited charm states is assumed to be negligible, hence $\lambda_{D \leftarrow D^*} = 0$. The same assumption holds for $D^*\pi$ correlation functions. In this case, however, the combinatorial background is already subtracted using the sidebandless approach described by Eq. (5) in Sec. III A. Therefore, the final model is given by Eq. (6), with $\lambda_{D \leftarrow D^*} = 0$ and $\lambda_{\text{SB}} = 0$.

To determine the free parameters related to $C_{\text{nonfemto}}(k^*)$, a background model is defined by imposing $C_{\text{gen}}(k^*) = 1$ in Eq. (6) for all pair combinations. The resulting expressions are fitted directly to the raw data in the range of $k^* \in [100, 600]$ MeV/c for $D\pi$ correlations and $k^* \in [200, 400]$ MeV/c for DK. The chosen fit range for correlations involving $D^*\pi$ is $k^* \in [300, 1000]$ MeV/c, while it is $k^* \in [250, 500]$ MeV/c for D^*K. The fit ranges are tuned to select a k^* region in which the femtoscopic correlations are expected to be negligible. The different sources of background, together with the total background model (violet band) and the raw data, are reported in the right panels of Figs. 2 and 3 for both the $D\pi$ and DK correlation functions, respectively. The blue band represents the residual $C_{\text{nonfemto}}(k^*)$, the orange band the combinatorial background $C_{\text{SB}}(k^*)$, and the red band the contribution arising from the feed down of D^{*+} to D^+, $C_{D \leftarrow D^*}(k^*)$. Once the parameters are fixed from the fit, the

genuine correlation function $C_{\mathrm{gen}}(k^*)$ is extracted from the raw data via Eq. (6), adapted to the pair of interest.

IV. SYSTEMATIC UNCERTAINTIES

The genuine correlation functions, which are the observables used to extract information on the residual strong final state interaction, are affected by several sources of systematic uncertainty related to the selection criteria or the background corrections to the raw data. Such uncertainty contributes to the systematic uncertainty of the scattering parameters, together with the systematic uncertainties associated with the source parameters and the choice of the fit range. The details on how the systematic uncertainties are estimated are provided in the following paragraphs.

A. Genuine correlation function

The choice of the selection criteria of the light-flavor and $D^{(*)}$-meson candidates determines the single-particle properties of the sample and hence the distributions of the pairs in the same (mixed) events. Therefore, an impact on the raw correlation function is expected, which is then propagated to the genuine correlation function. To estimate the systematic uncertainty associated with this contribution, the selection criteria mentioned in Sec. II are varied, and the raw correlation functions are recomputed for each set of variations. On the raw correlation function, the relative systematic uncertainty is below 3% in the case of $D^{(*)}K$ pairs and below 1% in the case of $D^{(*)}\pi$ pairs.

The uncertainties on the λ parameters, which affect the modeling of the background, are dominated by the uncertainty on the fraction of nonprompt charm mesons, D^+ mesons from D^{*+} decays, and light-flavor mesons from the decay of long-lived resonances as well as the purity of the $D^{(*)+}$ meson candidates. It is estimated by varying the fractions of charm mesons according to the uncertainties stated in Sec. II. The fractions of strongly-decaying long-lived resonances feeding into the light-flavor mesons, which are estimated using ThermalFist, are varied by 10% [79] and the purity of $D^{(*)+}$ mesons by 2% [54]. This leads to a variation of $\sim$10% of the λ-parameter values.

The systematic uncertainty on the background model is estimated by propagating the systematic uncertainties of the raw correlation functions and by varying the fractions according to the uncertainties stated above. Additionally, the fit range of the background model is varied in order to account for possible systematic effects related to the fit procedure. For particle pairs involving D^+ mesons, where the feed-down contribution from D^{*+} decays is modeled assuming Coulomb-only interaction, the uncertainty on the effective source parametrization, reported in Table II, represents an additional source of systematic uncertainty of the background model.

The total systematic uncertainty of the genuine correlation functions, computed taking into account all the contributions mentioned above, is found to be below 1% for opposite-charge Dπ, below 2% for same-charge Dπ, below 10% for same-charge DK, below 15% for opposite-charge DK, below 2.5% for $D^*\pi$, below 7% for same-charge D^*K, and below 25% for opposite-charge D^*K. In the low k^* region, the correlation functions are the most affected by the systematic uncertainties. The larger relative systematic uncertainty of the $D^{(*)}K$ correlation functions with respect to the ones of $D^{(*)}\pi$ arises from the propagated uncertainty of the raw correlation functions, which is related to the light-flavor meson selections. Overall, this represents the main source of systematic uncertainty of the genuine correlation functions, followed by the uncertainty on the λ parameters.

B. Scattering lengths

The systematic uncertainty associated to the extraction of the scattering lengths, discussed in the next section, besides the one related to the genuine correlation functions, is obtained by taking into account the choice of the fit range and the lack of precise knowledge of the source function. The first is estimated by varying the fit range by 50 MeV/c and the second one by performing the fit with different effective source parameters, determined according to the uncertainties reported in Table II. The latter represents the largest contribution to the systematic uncertainties on the scattering lengths, besides the propagated systematic uncertainties of the genuine correlation functions.

V. RESULTS

The measured genuine correlation functions, extracted from the raw data as described in Sec. III, are shown in Figs. 4 and 5 for correlations involving light-flavor and D^+ or D^{*+} mesons, respectively. In the femtoscopic region $k^* < 200$ MeV/c the genuine correlation functions are sensitive to the Coulomb and strong nuclear forces and can be compared to the corresponding calculations.

The strong interactions between the mesons depend on the quantum numbers of the systems and can therefore be separated into different isospin and strangeness configurations. These are namely: $D^{(*)}\pi(I = 3/2, 1/2, S = 0)$, $D^{(*)}\bar{K}(I = 1, 0, S = -1)$, and $D^{(*)}K(I = 0, S = +1)$. Several theoretical predictions are available for the Dπ and DK scattering lengths [89–93], while only two are present for the $D^*\pi$ and D^*K systems [93,94]. The models are listed below, together with a brief description of the calculation method. The corresponding scattering lengths are summarized in Tables IV and V.

(i) Liu *et al.* [89]: The S-wave scattering lengths $a_0^{\mathrm{D}\pi}(I = 3/2)$, $a_0^{\mathrm{D}\bar{K}}(I = 0)$, and $a_0^{\mathrm{D}\bar{K}}(I = 1)$ are calculated on the lattice using Lüschers finite volume technique. Extrapolation to the physical point is performed using unitarized chiral perturbation theory (ChPT) up to next-to-leading order (NLO), where the low-energy constants (LECs) are determined by a fit to the lattice data. The latter are
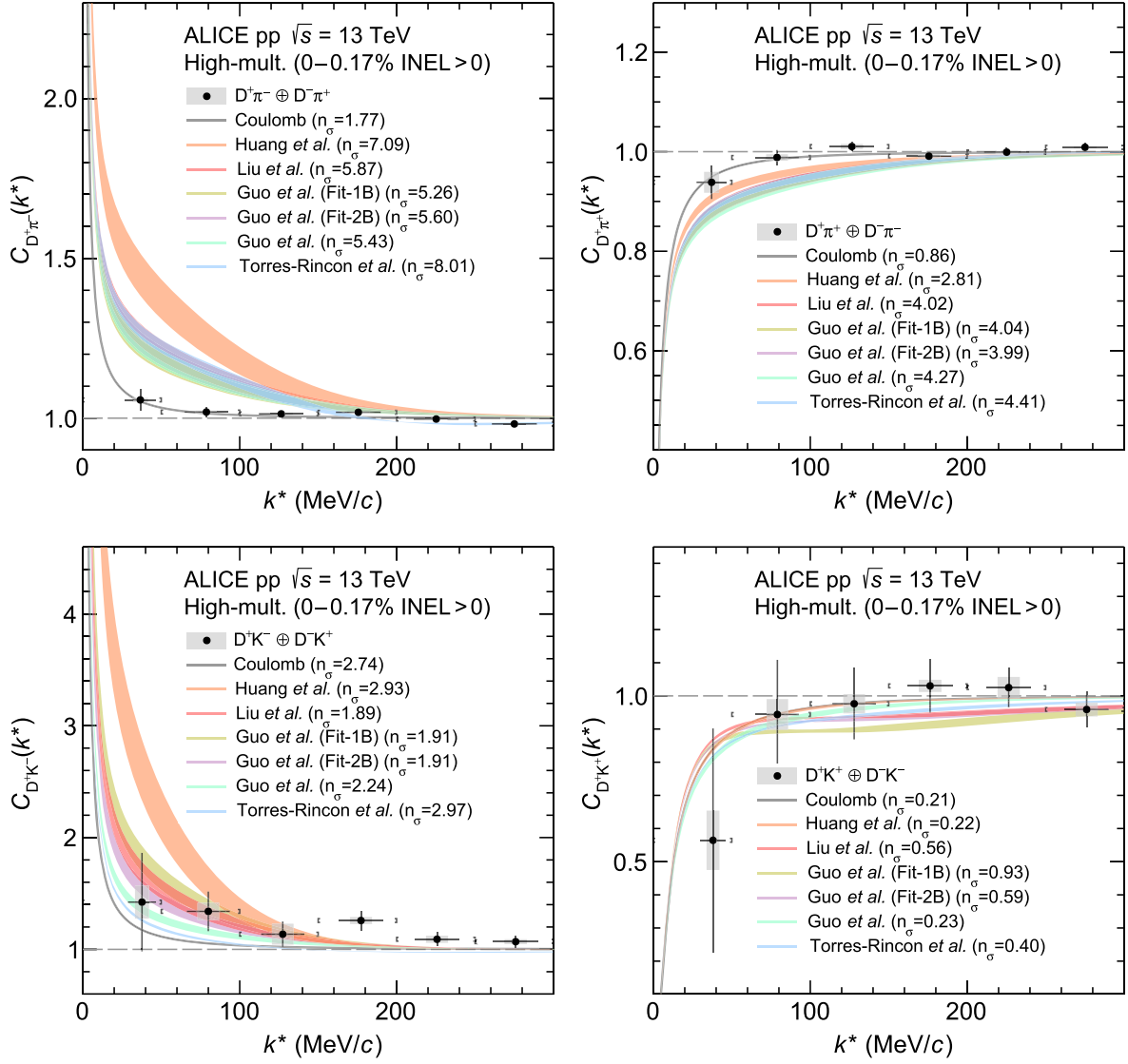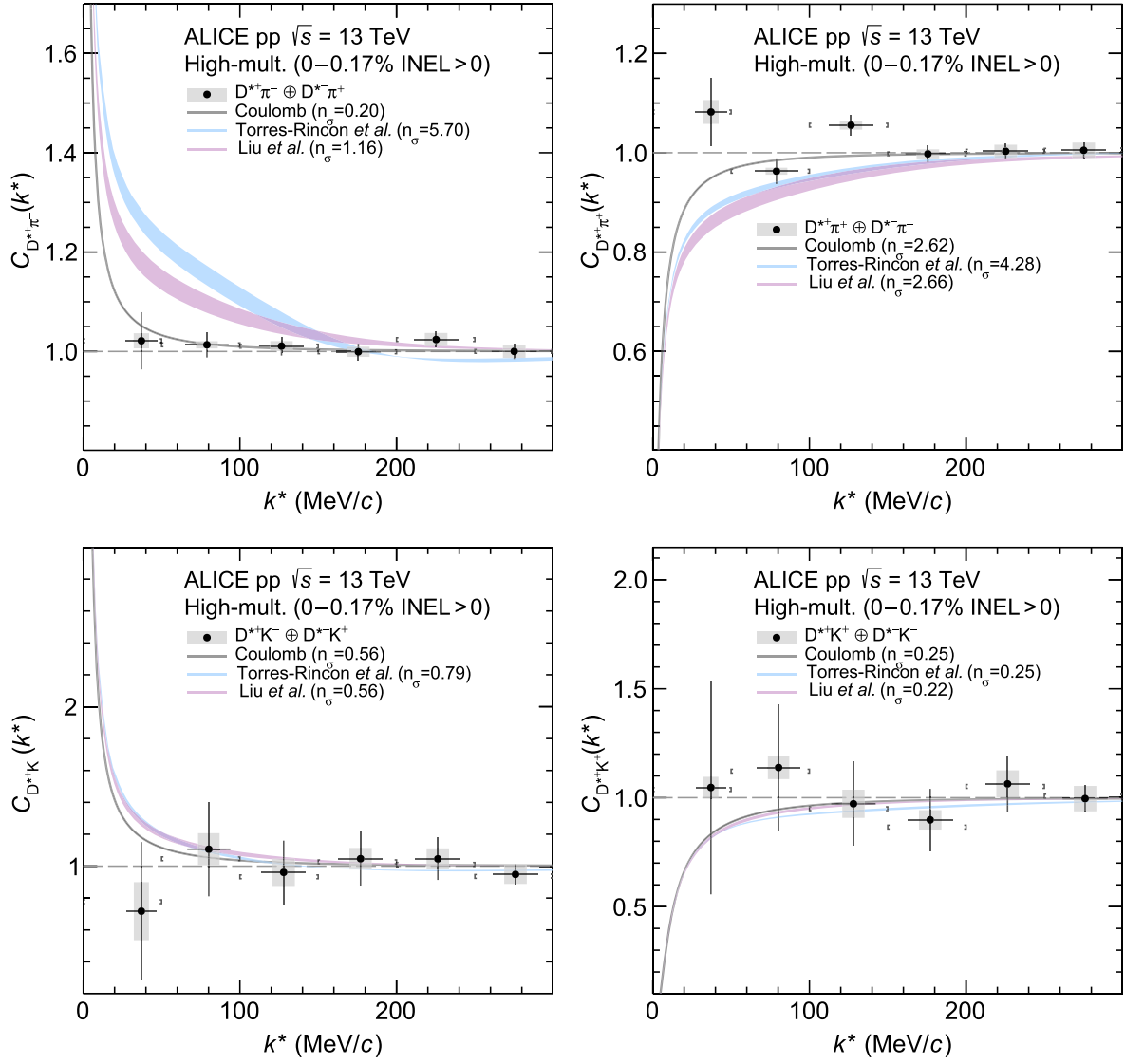
FIG. 4. Genuine correlation functions with statistical (bars) and systematic uncertainties (boxes) compared to theoretical model predictions (bands), listed in Tables IV and V. The width of the theoretical bands represents the uncertainty related to the source. The number of standard deviations n_σ is reported for each model in the legend. The results are shown for $D\pi$ (first row) and DK (second row) for the opposite- (left column) and same-charge (right column) combinations.

exploited to predict the scattering lengths in the other isospin channels.

(ii) Guo *et al.* [90]: N^3LO ChPT is employed and the LECs are determined by a global fit to lattice QCD data, including the S-wave scattering length from [89]. A chiral expansion scheme is applied to obtain the scattering lengths at physical pion mass.

(iii) Guo *et al.* [91]: The scattering length between the light-flavor and charmed mesons is obtained from unitarized ChPT up to NLO. The free parameters of the theory are constrained to lattice QCD calculations of the scattering length, including [89], and the finite-volume spectra. The fit is performed on different sets of the data, denoted as Fit-1B and Fit-2B.

Finally, the scattering lengths are obtained using a chiral extrapolation to the physical point.

(iv) Huang *et al.* [92]: Lattice QCD calculations of the finite-volume spectra and scattering lengths, including [89] are used to determine the LECs of the Lagrangian formulated within unitarized heavy-meson ChPT at N^3LO. The scattering lengths used in this paper are obtained from the iterated method.

(v) Torres-Rincon *et al.* [93]: The model employs unitarized ChPT with heavy-quark symmetry considerations at NLO, in a coupled-channel basis. The LECs at NLO are taken from [91]. Prediction for the $D^*\pi$ and D^*K scattering lengths are provided, exploiting heavy-quark spin symmetry.

FIG. 5. Genuine correlation functions with statistical (bars) and systematic uncertainties (boxes) compared to theoretical model predictions (bands). The width of the bands represents the uncertainty related to the source. The number of standard deviations n_σ is reported for each model in the legend. The results are shown for $D^*\pi$ (first row) and D^*K (second row) for the opposite- (left column) and same-charge (right column) combinations.

TABLE IV. Scattering lengths of the available theoretical models for the $D\pi$ interactions. The values are reported separately for the different isospin states.

Model		a_0 (fm)	
		$D\pi(I = 3/2)$	$D\pi(I = 1/2)$
Liu *et al.* [89]		-0.100 ± 0.002	$0.37^{+0.03}_{-0.02}$
Guo *et al.* [90]		-0.11	0.33
Guo *et al.* [91]	Fit-1B	$-0.101^{+0.005}_{-0.003}$	$0.31^{+0.01}_{-0.01}$
	Fit-2B	$-0.099^{+0.003}_{-0.004}$	$0.34^{+0.00}_{-0.03}$
Huang *et al.* [92]		-0.06 ± 0.02	0.61 ± 0.11
Torres-Rincon *et al.* [93]		-0.101	0.423
		$D^*\pi(I = 3/2)$	$D^*\pi(I = 1/2)$
Liu *et al.* [94]		$-0.13 - 0.00036i$	$0.27 - 0.00036i$

(vi) Liu *et al.* [94]: The S-wave scattering lengths of interactions involving the heavy vector meson D^* are derived within the framework of heavy-meson ChPT at N^2LO. The LECs at NLO are obtained from the mass splitting between heavy mesons and the resonance saturation model, while most of the N^2LO LECs are assumed to be negligible.

The theoretical curves of the Torres-Rincon *et al.* model were provided in a private communication with the authors and use the effective source parametrization $S_{eff}(r^*)$ described in Sec. III A, with values listed in Table II. In the other cases, the scattering lengths predicted by the models are converted into correlation functions by employing Eq. (4) with the effective source parametrization $S_{eff}(r^*)$. The wave function is obtained by taking into

TABLE V. Scattering lengths of the available theoretical models for the DK interactions. The values are reported separately for the different strangeness and isospin states. The real and imaginary components are associated with elastic and inelastic processes, respectively.

Model		a_0 (fm)		
		$DK(I=1)$	$D\bar{K}(I=1)$	$D\bar{K}(I=0)$
Liu *et al.* [89]		$0.07 \pm 0.03 + 0.17^{+0.02}_{-0.01}i$	-0.20 ± 0.01	$0.84^{+0.17}_{-0.22}$
Guo *et al.* [90]		-4.87×10^{-2}	-0.22	0.46
Guo *et al.* [91]	Fit-1B	$0.06^{+0.05}_{-0.03} + 0.30^{+0.09}_{-0.05}i$	$-0.18^{+0.01}_{-0.01}$	$0.96^{+1.44}_{-0.44}$
	Fit-2B	$0.05^{+0.04}_{-0.03} + 0.17^{+0.02}_{-0.03}i$	$-0.19^{+0.02}_{-0.02}$	$0.68^{+0.17}_{-0.16}$
Huang *et al.* [92]		-0.01 ± 0.03	-0.24 ± 0.02	1.81 ± 0.48
Torres-Rincon *et al.* [93]		$-0.027 + 0.083i$	-0.233	0.399
		$D^*K(I=1)$	$D^*\bar{K}(I=1)$	$D^*K(I=0)$
Liu *et al.* [94]		$-0.022 + 0.18i$	$-0.19 - 1.7 \times 10^{-6}i$	$0.29 + 5.2 \times 10^{-6}i$

account both the Coulomb and strong interaction. The former is modeled using the well-understood Coulomb potential, while the latter is parametrized with a Gaussian potential of the form

$$V(r) = V_0 \exp\left(-m_\rho^2 r^2\right), \tag{7}$$

where V_0 is the potential strength, and m_ρ is the mass of the lightest exchangeable meson, the ρ meson, which is the parameter that controls the potential range. The strength V_0 is tuned to reproduce the scattering lengths of the model [44].

The theoretical models provide the scattering parameters in the (strangeness, isospin) basis, but in the experiment, the interactions are accessible only in the charge basis. The same-charge pairs consist of a pure isospin state. The opposite-charge pairs are a mixture of two isospin states, which can be addressed by solving the coupled-channel Schrödinger equation with two isospin interaction components. In the case of $D^{(*)}\pi$ pairs, the isospin channel $I = 3/2$ is shared between the same- and opposite-charge configurations, as both have no net strangeness.

The theoretical correlation functions obtained from the different models of the strong interaction between charm and light-flavors mesons are compared to the measured genuine correlation functions in Figs. 4 and 5 for D^+ and D^{*+}, respectively. The predictions for the Coulomb-only hypothesis (gray curves) are shown as a reference, as any deviation of the experimental data from it indicates the presence of strong FSI. Additionally, the difference between the data and the calculations is quantified by the number of standard deviations n_σ and is reported in the figure legends. Each n_σ value is directly obtained from the p-value and reflects how well the specific model describes the data in the range of $k^* < 200$ MeV/c by considering the total uncertainty of the data as well as the predictions.

Even though the current statistical precision is not sufficient to distinguish between the individual model predictions of the residual strong interaction involving kaons, no tension with theory is observed in most cases.

The exception is $K^+D^- \oplus K^-D^+$, where the larger n_σ values are likely due to the fluctuation of the fourth data point. This is different for correlation functions involving pions. In the case of opposite-charge $D^{(*)}\pi$ pairs the data are significantly lower than any of the model predictions and clearly favor the Coulomb-only hypothesis. For same-charge pairs, the deviation between data and models is much smaller, however, the Coulomb-only hypothesis is still favored.

In general, the correlation functions for all the analyzed particle systems can be adequately described by only considering the Coulomb interaction, indicating a shallow residual strong interaction between the D^+ and D^{*+} mesons and light-flavor hadrons. A slight tension of $n_\sigma = 2.62$ is observed for the $D^{*+}\pi^+ \oplus D^{*-}\pi^-$ system, where the data points scatter around unity in the low k^* region. However, as mentioned above, the Coulomb-only hypothesis is still favored over the calculations with residual strong interactions. In the case of $D^+K^- \oplus D^-K^+$ the $n_\sigma = 2.72$ between the data, and Coulomb-only hypotheses could be related to the fluctuating data point at $k^* \sim 180$ MeV/c. By only considering smaller k^* values, the n_σ value reduces to 1.76, indicating that the Coulomb interaction sufficiently describes the measurement in the sensitive relative-momentum region.

The most precise correlation functions of this analysis, namely $D^+\pi^+ \oplus D^-\pi^-$ and $D^{*+}\pi^+ \oplus D^{*-}\pi^-$, are employed to extract the scattering length a_0 of the strong interaction. This is done by parametrizing the data using the same approach as for the theory predictions, which involves a Gaussian potential given by Eq. (7) with variable potential strength V_0 to model the strong interaction. As the isospin $I = 3/2$ state is shared among both charge combinations, the corresponding $V_0^{I=3/2}$ parameter is a common fit parameter of the two correlation functions. The potential strengths $V_0^{I=3/2}$ and $V_0^{I=1/2}$ are determined by a simultaneous χ^2 minimization within $k^* < 250$ MeV/c. Finally, the $I = 1/2$ and $3/2$ scattering lengths are calculated by solving the Schrödinger equation in the isospin basis.

The scattering lengths extracted by the minimization are summarized in Table VI. Figure 6 shows the corresponding model correlation functions (red bands) as well as the fitted data. The width of the bands represents the total uncertainty obtained from the χ^2 minimization. The χ^2/ndf of the combined fit of the $\mathrm{D}\pi$ correlation functions is 0.7 within $k^* < 250~\mathrm{MeV}/c$, while it is 1.0 in the case of $\mathrm{D}^*\pi$. The correlation between the scattering lengths for the isospin channels $I = 1/2$ and $I = 3/2$ extracted from the simultaneous fits are shown in Fig. 7. The red (orange) areas represent the confidence intervals for a 68% (95%) probability. Notably, the scattering lengths governing the residual strong interaction between D^+ and D^{*+} mesons with light-flavor mesons are found to be compatible with each other within the uncertainties. This is understood in

terms of heavy-quark spin symmetry, which states that, at leading order, the interaction of light-flavor mesons with pseudoscalar or vector charm mesons is the same. The measured scattering lengths for the isospin $I = 1/2$ channels are vanishing for both D^+ and D^{*+} mesons. In the case of $I = 3/2$, they are compatible with zero within uncertainties for the $\mathrm{D}\pi$ interaction, while they are positive with a significance of about 1.1σ for the $\mathrm{D}^*\pi$ interaction. The scattering lengths extracted from the data are further compared with the theoretical predictions reported in Tables IV and V. For the $I = 1/2$ channel, the measurements are significantly different from the values predicted by theoretical models, which cover the range between about 0.3 and 0.6 fm. Depending on the model, $5{-}13\sigma$ are obtained for $\mathrm{D}\pi$ and $6{-}8\sigma$ for $\mathrm{D}^*\pi$, taking into account the
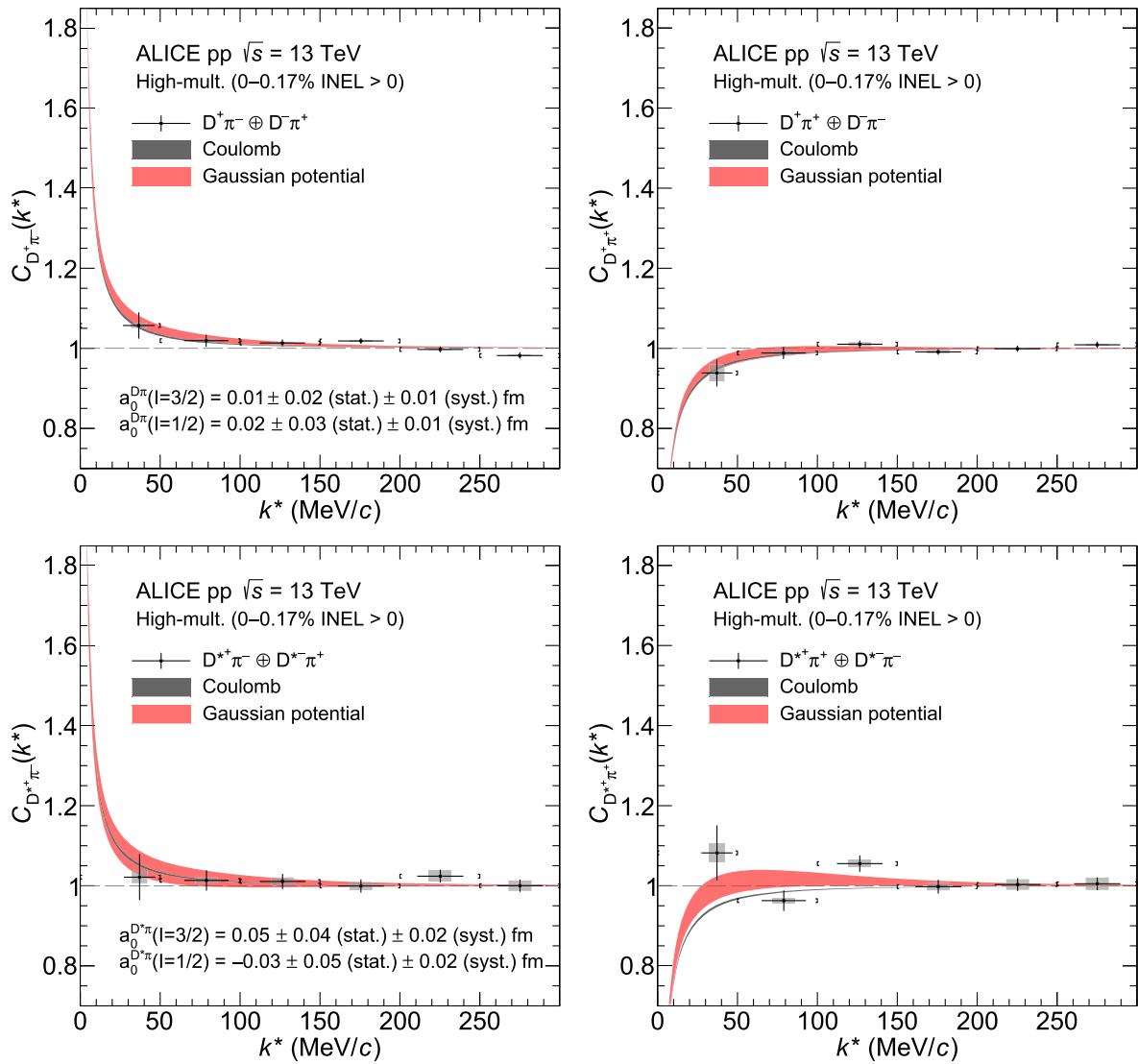
FIG. 6. Comparison of the $\mathrm{D}\pi$ (first row) and $\mathrm{D}^*\pi$ (second row) genuine correlation functions of same- (left column) and opposite-charge (right column) combinations with the results of the χ^2 minimization using a Gaussian potential to parametrize the strong interaction (red band). The width of the band corresponds to the total uncertainty. The gray curve represents the correlation functions assuming only interaction via the Coulomb force.
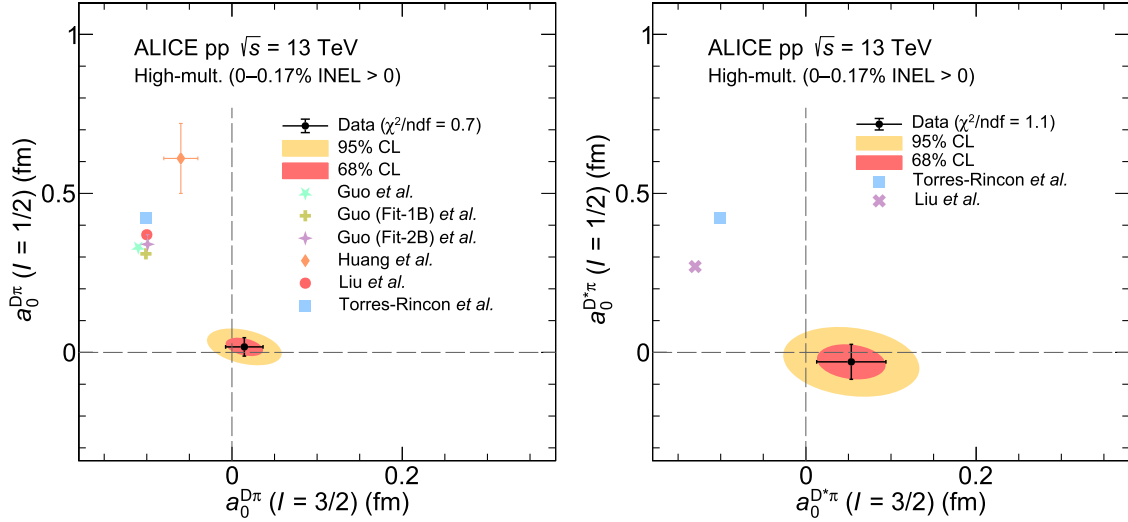
FIG. 7. Scattering length of the $D\pi$ (left) and $D^*\pi$ (right) interaction, for the two isospin channels that characterize the systems. They are extracted from a simultaneous χ^2 minimization to the experimental correlation functions. The red (orange) areas represent the resulting confidence intervals for a 68% (95%) probability. The dashed lines correspond to Coulomb interaction only, as the scattering lengths of the strong interaction vanish. As comparison, the available theoretical predictions [89–94], listed in Tables IV and V, are shown as well.

uncertainty of the data as well as the predictions. In the case of the $I = 3/2$ channel, the measurements also show a tension with the theoretical predictions, it is, however, smaller than in the $I = 1/2$ channel. In the $D\pi$ case, a deviation of 2–5σ is found, depending on the model, while it is around 3–4σ for $D^*\pi$. A much larger source size could diminish this discrepancy, as it leads to a less pronounced correlation signal for a given interaction strength. However, there is no obvious motivation for assuming a breaking of the universal m_T scaling of the core radius [78,79] in the case of correlation functions involving charm mesons. Especially, it is successfully used in the analysis of the experimental pD^- correlation function [54]. In Ref. [95] the hidden gauge formalism, implementing unitarization in coupled channels, is used to study the molecular nature of the lowest-lying D_1 states [$D_1(2420)$ and $D_1(2430)$], as well as the scattering amplitudes of some of the members of the meson-baryon basis considered ($D^*\pi$, $D\rho$) and the corresponding correlation functions. In order to better accommodate the $D_1(2430)$ within the experimental

observations [46,96], a bare quark-model pole structure is added explicitly, whose parameters dependence allows the authors to consider two plausible scenarios. The one denoted as Model B in their publication provides as a result a scattering length of $a_{D^*\pi}^{I=1/2} = 0.1$ fm, which is a value much closer to the one obtained in the present work. Alternatively, other complex structures, for example, in higher partial waves, not taken into account by the theory models, could modify the predictions.

In summary, the measured correlation functions between charm mesons and light-flavor mesons are compatible with the predictions obtained with only Coulomb interaction, suggesting that the residual strong interaction between these pairs of particles is shallow. A significant discrepancy in the $I = 1/2$ channel is found with respect to the predictions for the $D^{(*)}\pi$ scattering lengths, which is much less pronounced in the $I = 3/2$ channel. This discrepancy could be reconciled with the theory only in the case of a sizeable emitting source, which is not well motivated. The current precision of the $D^{(*)}K$ correlation functions does not allow for the discrimination between the available models and for a firm conclusion on the possible formation of bound states. Finally, the measured interactions suggest that the rescattering probability of charm mesons with light hadrons in the hadronic phase of the system produced in ultrarelativistic collisions is small. Even with values of scattering lengths predicted by theory calculations, which are larger than the measured ones reported in this article, a small impact on the D-meson final momenta is expected [62], given the duration of the hadronic phase of the system created in ultrarelativistic heavy-ion collisions of about $\Delta\tau_{\text{had}} \approx 5$–10 fm/$c$ [13,62,97].

TABLE VI. The scattering lengths a_0 of the $D^{(*)}\pi$ interaction, extracted from a χ^2 minimization to the experimental genuine correlation function, using a Gaussian potential to parametrize the strong interaction.

Pair	I	a_0 [fm]
$D\pi$	3/2	$0.01 \pm 0.02(\text{stat}) \pm 0.01(\text{syst})$
	1/2	$0.02 \pm 0.03(\text{stat}) \pm 0.01(\text{syst})$
$D^*\pi$	3/2	$0.05 \pm 0.04(\text{stat}) \pm 0.02(\text{syst})$
	1/2	$-0.03 \pm 0.05(\text{stat}) \pm 0.02(\text{syst})$

VI. CONCLUSION

The study of the residual strong interactions of $D^{(*)+}$ mesons with charged pions and kaons is performed for the first time, using high-multiplicity proton–proton collision data at $\sqrt{s} = 13$ TeV collected with the ALICE detector at the LHC. The femtoscopy technique is used to test various theoretical models of the strong interaction by comparing the experimental correlation functions for the different particle pairs with the predictions by theory. As comparison also the Coulomb-only assumption is tested and, within the current uncertainties, all the measured correlation functions can be well described by it. For the same charge $D^*\pi$ system, a slight tension with the Coulomb-only assumption of $n_\sigma = 2.62$ is observed. Still, it describes the data better than the model including the strong interaction. A comparison of the DK and D^*K data to theoretical predictions does not lead to a clear result, as no preference among the different models of the strong interaction or Coulomb-only hypothesis is observed due to the limited statistical precision. In the case of $D\pi$ interaction instead, the experimental data indicates that the theoretical models overestimate the scattering lengths, especially in the opposite-charge $D\pi$ correlation function, where a strong discrepancy is found. In comparison, Coulomb-only predictions yield a better description of the data. The same can be observed for the correlation functions involving D^{*+} mesons.

Among the experimental correlation functions studied in this work, the ones of the $D\pi$ and $D^*\pi$ systems are the most precise. Therefore, they are used to determine the scattering lengths of the strong interaction, which is modeled using a Gaussian potential. The scattering parameters are found to be small and compatible with zero. Especially, the disagreement between the scattering length of the isospin channel $I = 1/2$, extracted from the data, and the theoretical predictions is found to be larger than 5σ, challenging the current understanding of the residual strong interaction between D mesons and pions.

These findings also provide important information for the interpretation of the measurements of D-meson production and angular anisotropy in heavy-ion collisions [60,61] since they suggest that the effect of the rescattering of $D^{(*)+}$ mesons with light hadrons during the hadronic phase of the system produced in such collisions is small.

The precision of these measurements will improve with the data taken during the LHC Run 3 data-taking period. In fact, the dataset collected by the ALICE Collaboration will benefit from various detector upgrades, which include an improved spatial resolution crucial for the reconstruction of heavy-flavor decay vertices, and a larger luminosity thanks to the higher readout rate achievable [98]. Furthermore, with such improvements, the momentum correlation functions of other particle pairs involving charm hadrons will also become accessible.

[1] R. A. Arndt, W. J. Briscoe, I. I. Strakovsky, and R. L. Workman, Updated analysis of NN elastic scattering to 3 GeV, Phys. Rev. C **76,** 025209 (2007).

[2] R. Navarro Pérez, J. E. Amaro, and E. Ruiz Arriola, Partial wave analysis of nucleon–nucleon scattering below pion production threshold, Phys. Rev. C **88,** 024002 (2013); **88,** 069902(E) (2013).

[3] S. Pratt, Pion interferometry of quark–gluon plasma, Phys. Rev. D **33,** 1314 (1986).

[4] S. Acharya *et al.* (ALICE Collaboration), $p - p$, $p - \Lambda$ and Λ–Λ correlations studied via femtoscopy in pp reactions at $\sqrt{s} = 7$ TeV, Phys. Rev. C **99,** 024001 (2019).

[5] S. Acharya *et al.* (ALICE Collaboration), Scattering studies with low-energy kaon-proton femtoscopy in proton–proton collisions at the LHC, Phys. Rev. Lett. **124,** 092301 (2020).

[6] S. Acharya *et al.* (ALICE Collaboration), Exploring the $N\Lambda - N\Sigma$ coupled system with high precision correlation techniques at the LHC, Phys. Lett. B **833,** 137272 (2022).

[7] S. Acharya *et al.* (ALICE Collaboration), Investigation of the p – Σ^0 interaction via femtoscopy in pp collisions, Phys. Lett. B **805,** 135419 (2020).

[8] S. Acharya *et al.* (ALICE Collaboration), Study of the Λ–Λ interaction with femtoscopy correlations in pp and p–Pb collisions at the LHC, Phys. Lett. B **797,** 134822 (2019).

[9] S. Acharya *et al.* (ALICE Collaboration), First observation of an attractive interaction between a proton and a cascade baryon, Phys. Rev. Lett. **123,** 112002 (2019).

[10] ALICE Collaboration, Unveiling the strong interaction among hadrons at the LHC, Nature (London) **588,** 232 (2020); **590,** E13 (2021).

[11] S. Acharya *et al.* (ALICE Collaboration), Experimental evidence for an attractive p-ϕ interaction, Phys. Rev. Lett. **127,** 172301 (2021).

[12] S. Acharya *et al.* (ALICE Collaboration), Investigating the role of strangeness in baryon–antibaryon annihilation at the LHC, Phys. Lett. B **829,** 137060 (2022).

[13] ALICE Collaboration, The ALICE experiment—A journey through QCD, arXiv:2211.04384.

[14] S. Acharya *et al.* (ALICE Collaboration), Accessing the strong interaction between Λ baryons and charged kaons with the femtoscopy technique at the LHC, Phys. Lett. B **845,** 138145 (2023).

[15] B. Aubert *et al.* (*BABAR* Collaboration), Observation of a narrow meson decaying to $D_s^+\pi^0$ at a mass of 2.32 GeV/c^2, Phys. Rev. Lett. **90,** 242001 (2003).

[16] P. Krokovny *et al.* (Belle Collaboration), Observation of the $D_{SJ}(2317)$ and $D_{SJ}(2457)$ in B decays, Phys. Rev. Lett. **91,** 262002 (2003).

[17] D. Besson *et al.* (CLEO Collaboration), Observation of a narrow resonance of mass 2.46 GeV/c^2 decaying to $D_s^{*+}\pi^0$ and confirmation of the $D_{sJ}^*(2317)$ state, Phys. Rev. D **68,** 032002 (2003); **75,** 119908(E) (2007).

[18] S. Godfrey and N. Isgur, Mesons in a relativized quark model with chromodynamics, Phys. Rev. D **32,** 189 (1985).

[19] P. G. Ortega, J. Segovia, D. R. Entem, and F. Fernandez, Molecular components in P-wave charmed-strange mesons, Phys. Rev. D **94,** 074037 (2016).

[20] E. van Beveren and G. Rupp, Observed $D_s(2317)$ and tentative $D(2100 - 2300)$ as the charmed cousins of the light scalar nonet, Phys. Rev. Lett. **91,** 012003 (2003).

[21] S. Godfrey, Testing the nature of the $D_s(2317)^+$ and D(sJ)(2463)$^+$ states using radiative transitions, Phys. Lett. B **568,** 254 (2003).

[22] W. A. Bardeen, E. J. Eichten, and C. T. Hill, Chiral multiplets of heavy–light mesons, Phys. Rev. D **68,** 054024 (2003).

[23] Fayyazuddin and Riazuddin, Some comments on narrow resonances D_{s1}^* (2.46 GeV/c^2) and D_{s0} (2.317 GeV/c^2), Phys. Rev. D **69,** 114008 (2004).

[24] P. Colangelo and F. De Fazio, Understanding $D_{sJ}^*(2317)$, Phys. Lett. B **570,** 180 (2003).

[25] P. Colangelo, F. De Fazio, and A. Ozpineci, Radiative transitions of $D_{sJ}^*(2317)$ and $D_{sJ}(2460)$, Phys. Rev. D **72,** 074004 (2005).

[26] J. Lu, X.-L. Chen, W.-Z. Deng, and S.-L. Zhu, Pionic decays of $D_{sj}(2317)$, $D_{sj}(2460)$ and $B_{sj}(5718)$, $B_{sj}(5765)$, Phys. Rev. D **73,** 054012 (2006).

[27] T. Barnes, F. E. Close, and H. J. Lipkin, Implications of a DK molecule at 2.32 GeV, Phys. Rev. D **68,** 054006 (2003).

[28] A. P. Szczepaniak, Description of the $D_s * (2320)$ resonance as the D π atom, Phys. Lett. B **567,** 23 (2003).

[29] Y.-Q. Chen and X.-Q. Li, A comprehensive four-quark interpretation of $D_s(2317)$, $D_s(2457)$ and $D_s(2632)$, Phys. Rev. Lett. **93,** 232001 (2004).

[30] F.-K. Guo, P.-N. Shen, H.-C. Chiang, R.-G. Ping, and B.-S. Zou, Dynamically generated 0^+ heavy mesons in a heavy chiral unitary approach, Phys. Lett. B **641,** 278 (2006).

[31] F.-K. Guo, P.-N. Shen, and H.-C. Chiang, Dynamically generated 1^+ heavy mesons, Phys. Lett. B **647,** 133 (2007).

[32] H.-Y. Cheng and W.-S. Hou, B decays as spectroscope for charmed four quark states, Phys. Lett. B **566,** 193 (2003).

[33] M. E. Bracco, A. Lozea, R. D. Matheus, F. S. Navarra, and M. Nielsen, Disentangling two- and four-quark state pictures of the charmed scalar mesons, Phys. Lett. B **624,** 217 (2005).

[34] V. Dmitrasinovic, $D_{s0}^+(2317) - D_0(2308)$ mass difference as evidence for tetraquarks, Phys. Rev. Lett. **94,** 162002 (2005).

[35] T. E. Browder, S. Pakvasa, and A. A. Petrov, Comment on the new $D_s^{(*)+}\pi^0$ resonances, Phys. Lett. B **578,** 365 (2004).

[36] J. Vijande, F. Fernandez, and A. Valcarce, Open-charm meson spectroscopy, Phys. Rev. D **73,** 034002 (2006); **74,** 059903(E) (2006).

[37] S. K. Choi *et al.* (Belle Collaboration), Observation of a narrow charmonium-like state in exclusive $B^\pm \to K^\pm\pi^+\pi^- J/\psi$ decays, Phys. Rev. Lett. **91,** 262001 (2003).

[38] R. Aaij *et al.* (LHCb Collaboration), Observation of an exotic narrow doubly charmed tetraquark, Nat. Phys. **18,** 751 (2022).

[39] R. Aaij *et al.* (LHCb Collaboration), Study of the doubly charmed tetraquark T_{cc}^+, Nat. Commun. **13,** 3351 (2022).

[40] R. Aaij *et al.* (LHCb Collaboration), Observation of $J/\psi p$ resonances consistent with pentaquark states in $\Lambda_b^0 \to J/\psi K^- p$ decays, Phys. Rev. Lett. **115,** 072001 (2015).

[41] R. Aaij *et al.* (LHCb Collaboration), Observation of a narrow pentaquark state, $P_c(4312)^+$, and of two-peak structure of the $P_c(4450)^+$, Phys. Rev. Lett. **122,** 222001 (2019).

[42] H.-X. Chen, W. Chen, X. Liu, and S.-L. Zhu, The hidden-charm pentaquark and tetraquark states, Phys. Rep. **639,** 1 (2016).

[43] N. Brambilla, S. Eidelman, C. Hanhart, A. Nefediev, C.-P. Shen, C. E. Thomas, A. Vairo, and C.-Z. Yuan, The *XYZ* states: Experimental and theoretical status and perspectives, Phys. Rep. **873,** 1 (2020).

[44] Y. Kamiya, T. Hyodo, and A. Ohnishi, Femtoscopic study on DD* and D$\bar{D}^*$ interactions for T_{cc} and X(3872), Eur. Phys. J. A **58,** 131 (2022).

[45] N. Yalikun, Y.-H. Lin, F.-K. Guo, Y. Kamiya, and B.-S. Zou, Coupled-channel effects of the $\Sigma_c^{(*)}\bar{D}^{(*)} - \Lambda_c(2595)\bar{D}$ system and molecular nature of the P_c pentaquark states from one-boson exchange model, Phys. Rev. D **104,** 094039 (2021).

[46] K. Abe *et al.* (Belle Collaboration), Study of $B^- \to D^{**0}\pi^-(D^{**0} \to D^{(*)+}\pi^-)$ decays, Phys. Rev. D **69,** 112002 (2004).

[47] R. Aaij *et al.* (LHCb Collaboration), Dalitz plot analysis of $B^0 \to \bar{D}^0\pi^+\pi^-$ decays, Phys. Rev. D **92,** 032002 (2015).

[48] R. Aaij *et al.* (LHCb Collaboration), Amplitude analysis of $B^- \to D^+\pi^-\pi^-$ decays, Phys. Rev. D **94,** 072001 (2016).

[49] M.-L. Du, M. Albaladejo, P. Fernández-Soler, F.-K. Guo, C. Hanhart, U.-G. Meißner, J. Nieves, and D.-L. Yao, Towards a new paradigm for heavy-light meson spectroscopy, Phys. Rev. D **98,** 094018 (2018).

[50] M. Albaladejo, P. Fernandez-Soler, F.-K. Guo, and J. Nieves, Two-pole structure of the $D_0^*(2400)$, Phys. Lett. B **767,** 465 (2017).

[51] M.-L. Du, F.-K. Guo, C. Hanhart, B. Kubis, and U.-G. Meißner, Where is the lightest charmed scalar meson?, Phys. Rev. Lett. **126,** 192001 (2021).

[52] A. Asokan, M.-N. Tang, F.-K. Guo, C. Hanhart, Y. Kamiya, and U.-G. Meißner, Can the two-pole structure of the $D_0^*(2300)$ be understood from recent lattice data?, Eur. Phys. J. C **83,** 850 (2023).

[53] M. Albaladejo, J. Nieves, and E. Ruiz-Arriola, Femtoscopic signatures of the lightest S-wave scalar open-charm mesons, Phys. Rev. D **108,** 014020 (2023).

[54] S. Acharya *et al.* (ALICE Collaboration), First study of the two-body scattering involving charm hadrons, Phys. Rev. D **106,** 052010 (2022).

[55] P. Braun-Munzinger, V. Koch, T. Schäfer, and J. Stachel, Properties of hot and dense matter from relativistic heavy ion collisions, Phys. Rep. **621,** 76 (2016).

[56] J. Adams *et al.* (STAR Collaboration), Experimental and theoretical challenges in the search for the quark-gluon plasma: The STAR Collaboration's critical assessment of the evidence from RHIC collisions, Nucl. Phys. **A757,** 102 (2005).

[57] B. B. Back *et al.* (PHOBOS Collaboration), The PHOBOS perspective on discoveries at RHIC, Nucl. Phys. **A757,** 28 (2005).

[58] K. Adcox *et al.* (PHENIX Collaboration), Formation of dense partonic matter in relativistic nucleus-nucleus collisions at RHIC: Experimental evaluation by the PHENIX collaboration, Nucl. Phys. **A757,** 184 (2005).

[59] I. Arsene *et al.* (BRAHMS Collaboration), Quark-gluon plasma and color glass condensate at RHIC? The perspective from the BRAHMS experiment, Nucl. Phys. **A757,** 1 (2005).

[60] S. Acharya *et al.* (ALICE Collaboration), Transverse-momentum and event-shape dependence of D-meson flow

harmonics in Pb–Pb collisions at $\sqrt{s_{NN}} = 5.02$ TeV, Phys. Lett. B **813,** 136054 (2021).

[61] S. Acharya *et al.* (ALICE Collaboration), Prompt D^0, D^+, and D^{*+} production in Pb–Pb collisions at $\sqrt{s_{NN}} = 5.02$ TeV, J. High Energy Phys. 01 (2022) 174.

[62] M. He, R. J. Fries, and R. Rapp, Thermal relaxation of charm in hadronic matter, Phys. Lett. B **701,** 445 (2011).

[63] ALICE Collaboration, Performance of the ALICE V0 system, J. Instrum. **8,** P10016 (2013).

[64] K. Aamodt *et al.* (ALICE Collaboration), Alignment of the ALICE inner tracking system with cosmic-ray tracks, J. Instrum. **5,** P03003 (2010).

[65] J. Alme, Y. Andres, H. Appelshäuser, S. Bablok, N. Bialas *et al.*, The ALICE TPC, a large 3-dimensional tracking device with fast readout for ultra-high multiplicity events, Nucl. Instrum. Methods Phys. Res., Sect. A **622,** 316 (2010).

[66] A. Akindinov *et al.*, Performance of the ALICE time-of-flight detector at the LHC, Eur. Phys. J. Plus **128,** 44 (2013).

[67] T. Sjöstrand, S. Ask, J. R. Christiansen, R. Corke, N. Desai, P. Ilten, S. Mrenna, S. Prestel, C. O. Rasmussen, and P. Z. Skands, An introduction to PYTHIA 8.2, Comput. Phys. Commun. **191,** 159 (2015).

[68] R. Brun, A. McPherson, P. Zanarini, M. Maire, and F. Bruyant, Geant 3: User's guide Geant 3.10, Geant 3.11, Technical Report, CERN, 1987, https://cds.cern.ch/record/1119728.

[69] K. Aamodt *et al.* (ALICE Collaboration), The ALICE experiment at the CERN LHC, J. Instrum. **3,** S08002 (2008).

[70] ALICE Collaboration, The ALICE definition of primary particles, ALICE-PUBLIC-2017-005, 2017, https://cds.cern.ch/record/2270008.

[71] V. Vovchenko and H. Stoecker, Thermal-Fist: A package for heavy-ion collisions and hadronic equation of state, Comput. Phys. Commun. **244,** 295 (2019).

[72] R. L. Workman *et al.* (Particle Data Group), Review of particle physics, Prog. Theor. Exp. Phys. **2022** (2022) 083C01.

[73] T. Chen and C. Guestrin, XGBoost: A scalable tree boosting system, in *KDD '16: The 22nd ACM SIGKDD International Conference on Knowledge Discovery and Data Mining, San Francisco, California, USA* (Association for Computing Machinery, New York, NY, 2016).

[74] L. Barioglio, F. Catalano, M. Concas, P. Fecchio, F. Grosa, F. Mazzaschi, and M. Puccio, Minimal heavy-ion physics environment for machine learning program library, hipe4ml/hipe4ml, 10.5281/zenodo.7014886 (2022).

[75] S. Acharya *et al.* (ALICE Collaboration), Measurement of beauty and charm production in pp collisions at $\sqrt{s} = 5.02$ TeV via non-prompt and prompt D mesons, J. High Energy Phys. 05 (2021) 220.

[76] S. Acharya *et al.* (ALICE Collaboration), Measurement of D^0, D^+, D^{*+} and D_s^+ production in pp collisions at $\sqrt{s} = 5.02$ TeV with ALICE, Eur. Phys. J. C **79,** 388 (2019).

[77] M. A. Lisa, S. Pratt, R. Soltz, and U. Wiedemann, Femto-scopy in relativistic heavy ion collisions, Annu. Rev. Nucl. Part. Sci. **55,** 357 (2005).

[78] S. Acharya *et al.* (ALICE Collaboration), Search for a common baryon source in high-multiplicity pp collisions at the LHC, Phys. Lett. B **811,** 135849 (2020).

[79] S. Acharya *et al.* (ALICE Collaboration), Common femto-scopic hadron-emission source in pp collisions at the LHC, arXiv:2311.14527.

[80] S. Acharya *et al.* (ALICE Collaboration), Constraining the $\bar{K}N$ coupled channel dynamics using femtoscopic correlations at the LHC, Eur. Phys. J. C **83,** 340 (2023).

[81] D. L. Mihaylov, V. Mantovani Sarti, O. W. Arnold, L. Fabbietti, B. Hohlweger, and A. M. Mathis, A femtosc opic correlation analysis tool using the Schrödinger equation (CATS), Eur. Phys. J. C **78,** 394 (2018).

[82] R. Del Grande, L. Šerkšnytė, L. Fabbietti, V. M. Sarti, and D. Mihaylov, A method to remove lower order contributions in multi-particle femtoscopic correlation functions, Eur. Phys. J. C **82,** 244 (2022).

[83] F. E. James, Monte Carlo phase space, CERN Academic Training Lecture, CERN, Geneva, 1968, https://cds.cern.ch/record/275743.

[84] B. Abelev *et al.* (ALICE Collaboration), $K_S^0 K_S^0$ correlations in pp collisions at $\sqrt{s} = 7$ TeV from the LHC ALICE experiment, Phys. Lett. B **717,** 151 (2012).

[85] B. Abelev *et al.* (ALICE Collaboration), Charged kaon femtoscopic correlations in pp collisions at $\sqrt{s} = 7$ TeV, Phys. Rev. D **87,** 052016 (2013).

[86] K. Aamodt *et al.* (ALICE Collaboration), Femtoscopy of pp collisions at $\sqrt{s} = 0.9$ and 7 TeV at the LHC with two-pion Bose–Einstein correlations, Phys. Rev. D **84,** 112004 (2011).

[87] J. Adam *et al.* (ALICE Collaboration), Two-pion femto-scopy in p–Pb collisions at $\sqrt{s_{NN}} = 5.02$ TeV, Phys. Rev. C **91,** 034906 (2015).

[88] J. Adam *et al.* (ALICE Collaboration), Insight into particle production mechanisms via angular correlations of identi-fied particles in pp collisions at $\sqrt{s} = 7$ TeV, Eur. Phys. J. C **77,** 569 (2017); **79,** 998(E) (2019).

[89] L. Liu, K. Orginos, F.-K. Guo, C. Hanhart, and U.-G. Meissner, Interactions of charmed mesons with light pseu-doscalar mesons from lattice QCD and implications on the nature of the $D_{s0}^*(2317)$, Phys. Rev. D **87,** 014508 (2013).

[90] X.-Y. Guo, Y. Heo, and M. F. M. Lutz, On chiral extrapo-lations of charmed meson masses and coupled-channel reaction dynamics, Phys. Rev. D **98,** 014510 (2018).

[91] Z.-H. Guo, L. Liu, U.-G. Meißner, J. A. Oller, and A. Rusetsky, Towards a precise determination of the scattering amplitudes of the charmed and light-flavor pseudoscalar mesons, Eur. Phys. J. C **79,** 13 (2019).

[92] B.-L. Huang, Z.-Y. Lin, and S.-L. Zhu, Light pseudoscalar meson and heavy meson scattering lengths to O(p4) in heavy meson chiral perturbation theory, Phys. Rev. D **105,** 036016 (2022).

[93] J. M. Torres-Rincon, A. Ramos, and L. Tolos, Femtoscopy of D mesons and light mesons upon unitarized effective field theories, Phys. Rev. D **108,** 096008 (2023).

[94] Z.-W. Liu, Y.-R. Liu, X. Liu, and S.-L. Zhu, Pseudoscalar meson and heavy vector meson scattering lengths, Phys. Rev. D **84,** 034002 (2011).

[95] K. P. Khemchandani, L. M. Abreu, A. Martinez Torres, and F. S. Navarra, Can femtoscopic correlation function shed light on the nature of the lightest, charm, axial mesons?, arXiv:2312.11811.

[96] R. Aaij *et al.* (LHCb Collaboration), Amplitude analysis of $B^0 \to \bar{D}^0 K^+ \pi^-$ decays, Phys. Rev. D **92**, 012012 (2015).

[97] L. M. Abreu, D. Cabrera, F. J. Llanes-Estrada, and J. M. Torres-Rincon, Charm diffusion in a pion gas implementing unitarity, chiral and heavy quark symmetries, Ann. Phys. (N.Y.) **326**, 2737 (2011).

[98] ALICE Collaboration, ALICE upgrades during the LHC long shutdown 2, J. Instrum. **19**, P05062 (2024).

S. Acharya[129] D. Adamová[87] G. Aglieri Rinella[33] L. Aglietta[25] M. Agnello[30] N. Agrawal[26] Z. Ahammed[137] S. Ahmad[16] S. U. Ahn[72] I. Ahuja[38] A. Akindinov[143] V. Akishina[39] M. Al-Turany[98] D. Aleksandrov[143] B. Alessandro[57] H. M. Alfanda[6] R. Alfaro Molina[68] B. Ali[16] A. Alici[26] N. Alizadehvandchali[118] A. Alkin[106] J. Alme[21] G. Alocco[53] T. Alt[65] A. R. Altamura[51] I. Altsybeev[96] J. R. Alvarado[45] M. N. Anaam[6] C. Andrei[46] N. Andreou[117] A. Andronic[128] E. Andronov[143] V. Anguelov[95] F. Antinori[55] P. Antonioli[52] N. Apadula[75] L. Aphecetche[105] H. Appelshäuser[65] C. Arata[74] S. Arcelli[26] M. Aresti[23] R. Arnaldi[57] J. G. M. C. A. Arneiro[112] I. C. Arsene[20] M. Arslandok[140] A. Augustinus[33] R. Averbeck[98] M. D. Azmi[16] H. Baba[126] A. Badalà[54] J. Bae[106] Y. W. Baek[41] X. Bai[122] R. Bailhache[65] Y. Bailung[49] R. Bala[92] A. Balbino[30] A. Baldisseri[132] B. Balis[2] D. Banerjee[4] Z. Banoo[92] F. Barile[32] L. Barioglio[57] M. Barlou[79] B. Barman[42] G. G. Barnaföldi[47] L. S. Barnby[117] E. Barreau[105] V. Barret[129] L. Barreto[112] C. Bartels[121] K. Barth[33] E. Bartsch[65] N. Bastid[129] S. Basu[76] G. Batigne[105] D. Battistini[96] B. Batyunya[144] D. Bauri[48] J. L. Bazo Alba[103] I. G. Bearden[84] C. Beattie[140] P. Becht[98] D. Behera[49] I. Belikov[131] A. D. C. Bell Hechavarria[128] F. Bellini[26] R. Bellwied[118] S. Belokurova[143] L. G. E. Beltran[111] Y. A. V. Beltran[45] G. Bencedi[47] A. Bensaoula[118] S. Beole[25] Y. Berdnikov[143] A. Berdnikova[95] L. Bergmann[95] M. G. Besoiu[64] L. Betev[33] P. P. Bhaduri[137] A. Bhasin[92] M. A. Bhat[4] B. Bhattacharjee[42] L. Bianchi[25] N. Bianchi[50] J. Bielčík[36] J. Bielčíková[87] A. P. Bigot[131] A. Bilandzic[96] G. Biro[47] S. Biswas[4] N. Bize[105] J. T. Blair[110] D. Blau[143] M. B. Blidaru[98] N. Bluhme[39] C. Blume[65] G. Boca[22,56] F. Bock[88] T. Bodova[21] J. Bok[17] L. Boldizsár[47] M. Bombara[38] P. M. Bond[33] G. Bonomi[56,136] H. Borel[132] A. Borissov[143] A. G. Borquez Carcamo[95] H. Bossi[140] E. Botta[25] Y. E. M. Bouziani[65] L. Bratrud[65] P. Braun-Munzinger[98] M. Bregant[112] M. Broz[36] G. E. Bruno[32,97] M. D. Buckland[24] D. Budnikov[143] H. Buesching[65] S. Bufalino[30] P. Buhler[104] N. Burmasov[143] Z. Buthelezi[69,125] A. Bylinkin[21] S. A. Bysiak[109] J. C. Cabanillas Noris[111] M. F. T. Cabrera[118] M. Cai[6] H. Caines[140] A. Caliva[29] E. Calvo Villar[103] J. M. M. Camacho[111] P. Camerini[24] F. D. M. Canedo[112] S. L. Cantway[140] M. Carabas[115] A. A. Carballo[33] F. Carnesecchi[33] R. Caron[130] L. A. D. Carvalho[112] J. Castillo Castellanos[132] M. Castoldi[33] F. Catalano[25,33] S. Cattaruzzi[24] C. Ceballos Sanchez[144] R. Cerri[25] I. Chakaberia[75] P. Chakraborty[48,138] S. Chandra[137] S. Chapeland[33] M. Chartier[121] S. Chattopadhyay[137] S. Chattopadhyay[101] T. Cheng[6,98] C. Cheshkov[130] V. Chibante Barroso[33] D. D. Chinellato[113] E. S. Chizzali[96,‡] J. Cho[59] S. Cho[59] P. Chochula[33] D. Choudhury[42] P. Christakoglou[85] C. H. Christensen[84] P. Christiansen[76] T. Chujo[127] M. Ciacco[30] C. Cicalo[53] M. R. Ciupek[98] G. Clai[52,§] F. Colamaria[51] J. S. Colburn[102] D. Colella[32,97] M. Colocci[26] M. Concas[33] G. Conesa Balbastre[74] Z. Conesa del Valle[133] G. Contin[24] J. G. Contreras[36] M. L. Coquet[105,132] P. Cortese[57,135] M. R. Cosentino[114] F. Costa[33] S. Costanza[22,56] C. Cot[133] J. Crkovská[95] P. Crochet[129] R. Cruz-Torres[75] P. Cui[6] A. Dainese[55] G. Dange[39] M. C. Danisch[95] A. Danu[64] P. Das[81] P. Das[4] S. Das[4] A. R. Dash[128] S. Dash[48] A. De Caro[29] G. de Cataldo[51] J. de Cuveland[39] A. De Falco[23] D. De Gruttola[29] N. De Marco[57] C. De Martin[24] S. De Pasquale[29] R. Deb[136] R. Del Grande[96] L. Dello Stritto[33] W. Deng[6] K. C. Devereaux[19] P. Dhankher[19] D. Di Bari[32] A. Di Mauro[33] B. Diab[132] R. A. Diaz[7,144] T. Dietel[116] Y. Ding[6] J. Ditzel[65] R. Divià[33] D. U. Dixit[19] Ø. Djuvsland[21] U. Dmitrieva[143] A. Dobrin[64] B. Dönigus[65] J. M. Dubinski[138] A. Dubla[98] S. Dudi[91] P. Dupieux[129] N. Dzalaiova[13] T. M. Eder[128] R. J. Ehlers[75] F. Eisenhut[65] R. Ejima[93] D. Elia[51] B. Erazmus[105] F. Ercolessi[26] B. Espagnon[133] G. Eulisse[33] D. Evans[102] S. Evdokimov[143] L. Fabbietti[96] M. Faggin[28] J. Faivre[74] F. Fan[6] W. Fan[75] A. Fantoni[50] M. Fasel[88] A. Feliciello[57] G. Feofilov[143] A. Fernández Téllez[45] L. Ferrandi[112] M. B. Ferrer[33] A. Ferrero[132] C. Ferrero[57,∥] A. Ferretti[25] V. J. G. Feuillard[95] V. Filova[36] D. Finogeev[143] F. M. Fionda[53] E. Flatland[33] F. Flor[118] A. N. Flores[110] S. Foertsch[69] I. Fokin[95] S. Fokin[143] U. Follo[57,∥] E. Fragiacomo[58] E. Frajna[47] U. Fuchs[33] N. Funicello[29]

C. Furget [74], A. Furs [143], T. Fusayasu [100], J. J. Gaardhøje [84], M. Gagliardi [25], A. M. Gago [103], T. Gahlaut,[48]
C. D. Galvan [111], D. R. Gangadharan [118], P. Ganoti [79], C. Garabatos [98], T. García Chávez [45], E. Garcia-Solis,[9]
C. Gargiulo [33], P. Gasik [98], H. M. Gaur,[39] A. Gautam [120], M. B. Gay Ducati [67], M. Germain [105], A. Ghimouz,[127]
C. Ghosh,[137] M. Giacalone [52], G. Gioachin [30], P. Giubellino [57,98], P. Giubilato [28], A. M. C. Glaenzer [132], P. Glässel [95],
E. Glimos [124], D. J. Q. Goh,[77] V. Gonzalez [139], P. Gordeev [143], M. Gorgon [2], K. Goswami [49], S. Gotovac,[34]
V. Grabski [68], L. K. Graczykowski [138], E. Grecka [87], A. Grelli [60], C. Grigoras [33], V. Grigoriev [143], S. Grigoryan [1,144],
F. Grosa [33], J. F. Grosse-Oetringhaus [33], R. Grosso [98], D. Grund [36], N. A. Grunwald,[95] G. G. Guardiano [113],
R. Guernane [74], M. Guilbaud [105], K. Gulbrandsen [84], T. Gündem [65], T. Gunji [126], W. Guo [6], A. Gupta [92],
R. Gupta [92], R. Gupta [49], K. Gwizdziel [138], L. Gyulai [47], C. Hadjidakis [133], F. U. Haider [92], S. Haidlova [36],
M. Haldar,[4] H. Hamagaki [77], A. Hamdi [75], Y. Han [141], B. G. Hanley [139], R. Hannigan [110], J. Hansen [76],
J. W. Harris [140], A. Harton [9], M. V. Hartung [65], H. Hassan [119], D. Hatzifotiadou [52], P. Hauer [43], L. B. Havener [140],
E. Hellbär [98], H. Helstrup [35], M. Hemmer [65], T. Herman [36], S. G. Hernandez,[118] G. Herrera Corral [8], F. Herrmann,[128]
S. Herrmann [130], K. F. Hetland [35], B. Heybeck [65], H. Hillemanns [33], B. Hippolyte [131], F. W. Hoffmann [71],
B. Hofman [60], G. H. Hong [141], M. Horst [96], A. Horzyk [2], Y. Hou [6], P. Hristov [33], P. Huhn,[65] L. M. Huhta [119],
T. J. Humanic [89], A. Hutson [118], D. Hutter [39], M. C. Hwang [19], R. Ilkaev,[143] H. Ilyas [14], M. Inaba [127],
G. M. Innocenti [33], M. Ippolitov [143], A. Isakov [85], T. Isidori [120], M. S. Islam [101], M. Ivanov [13], M. Ivanov [98],
V. Ivanov [143], K. E. Iversen [76], M. Jablonski [2], B. Jacak [19,75], N. Jacazio [26], P. M. Jacobs [75], S. Jadlovska,[108]
J. Jadlovsky,[108] S. Jaelani [83], C. Jahnke [112], M. J. Jakubowska [138], M. A. Janik [138], T. Janson,[71] S. Ji [17], S. Jia [10],
A. A. P. Jimenez [66], F. Jonas [75,88,128], D. M. Jones [121], J. M. Jowett [33,98], J. Jung [65], M. Jung [65], A. Junique [33],
A. Jusko [102], J. Kaewjai,[107] P. Kalinak [61], A. Kalweit [33], Y. Kamiya [99,¶], A. Karasu Uysal [73,**], D. Karatovic [90],
O. Karavichev [143], T. Karavicheva [143], E. Karpechev [143], M. J. Karwowska [33,138], U. Kebschull [71], R. Keidel [142],
D. L. D. Keijdener [60], M. Keil [33], B. Ketzer [43], S. S. Khade [49], A. M. Khan [122], S. Khan [16], A. Khanzadeev [143],
Y. Kharlov [143], A. Khatun [120], A. Khuntia [36], Z. Khuranova [65], B. Kileng [35], B. Kim [106], C. Kim [17], D. J. Kim [119],
E. J. Kim [70], J. Kim [141], J. Kim [59], J. Kim [70], M. Kim [19], S. Kim [18], T. Kim [141], K. Kimura [93], A. Kirkova [37],
S. Kirsch [65], I. Kisel [39], S. Kiselev [143], A. Kisiel [138], J. P. Kitowski [2], J. L. Klay [5], J. Klein [33], S. Klein [75],
C. Klein-Bösing [128], M. Kleiner [65], T. Klemenz [96], A. Kluge [33], C. Kobdaj [107], T. Kollegger,[98] A. Kondratyev [144],
N. Kondratyeva [143], J. Konig [65], S. A. Konigstorfer [96], P. J. Konopka [33], G. Kornakov [138], M. Korwieser [96],
S. D. Koryciak [2], A. Kotliarov [87], N. Kovacic [90], V. Kovalenko [143], M. Kowalski [109], V. Kozhuharov [37], I. Králik [61],
A. Kravčáková [38], L. Krcal [33,39], M. Krivda [61,102], F. Krizek [87], K. Krizkova Gajdosova [33], C. Krug [67], M. Krüger [65],
D. M. Krupova [36], E. Kryshen [143], V. Kučera [59], C. Kuhn [131], P. G. Kuijer [85], T. Kumaoka,[127] D. Kumar,[137]
L. Kumar [91], N. Kumar,[91] S. Kumar [32], S. Kundu [33], P. Kurashvili [80], A. Kurepin [143], A. B. Kurepin [143],
A. Kuryakin [143], S. Kushpil [87], V. Kuskov [143], M. Kutyla,[138] M. J. Kweon [59], Y. Kwon [141], S. L. La Pointe [39],
P. La Rocca [27], A. Lakrathok,[107] M. Lamanna [33], A. R. Landou [74], R. Langoy [123], P. Larionov [33], E. Laudi [33],
L. Lautner [33,96], R. A. N. Laveaga,[111] R. Lavicka [104], R. Lea [56,136], H. Lee [106], I. Legrand [46], G. Legras [128],
J. Lehrbach [39], T. M. Lelek,[2] R. C. Lemmon [86], I. León Monzón [111], M. M. Lesch [96], E. D. Lesser [19], P. Lévai [47],
X. Li,[10] B. E. Liang-gilman [19], J. Lien [123], R. Lietava [102], I. Likmeta [118], B. Lim [25], S. H. Lim [17], V. Lindenstruth [39],
A. Lindner,[46] C. Lippmann [98], D. H. Liu [6], J. Liu [121], G. S. S. Liveraro [113], I. M. Lofnes [21], C. Loizides [88],
S. Lokos [109], J. Lömker [60], P. Loncar [34], X. Lopez [129], E. López Torres [7], P. Lu [98,122], F. V. Lugo [68], J. R. Luhder [128],
M. Lunardon [28], G. Luparello [58], Y. G. Ma [40], M. Mager [33], A. Maire,[131] E. M. Majerz,[2] M. V. Makariev [37],
M. Malaev [143], G. Malfattore [26], N. M. Malik [92], Q. W. Malik,[20] S. K. Malik [92], L. Malinina [144,†,††], D. Mallick [133],
N. Mallick [49], G. Mandaglio [31,54], S. K. Mandal [80], A. Manea [64], V. Manko [143], F. Manso [129], V. Manzari [51],
Y. Mao [6], R. W. Marcjan [2], G. V. Margagliotti [24], A. Margotti [52], A. Marín [98], C. Markert [110], P. Martinengo [33],
M. I. Martínez [45], G. Martínez García [105], M. P. P. Martins [112], S. Masciocchi [98], M. Masera [25], A. Masoni [53],
L. Massacrier [133], O. Massen [60], A. Mastroserio [51,134], O. Matonoha [76], S. Mattiazzo [28], A. Matyja [109], C. Mayer [109],
A. L. Mazuecos [33], F. Mazzaschi [25], M. Mazzilli [33], J. E. Mdhluli [125], Y. Melikyan [44], A. Menchaca-Rocha [68],
J. E. M. Mendez [66], E. Meninno [104], A. S. Menon [118], M. W. Menzel,[33,95] M. Meres [13], Y. Miake [127], L. Micheletti [33],
D. L. Mihaylov [96], K. Mikhaylov [143,144], N. Minafra [120], D. Miśkowiec [98], A. Modak [4], B. Mohanty,[81]
M. Mohisin Khan [16,‡], M. A. Molander [44], S. Monira [138], C. Mordasini [119], D. A. Moreira De Godoy [128],
I. Morozov [143], A. Morsch [33], T. Mrnjavac [33], V. Muccifora [50], S. Muhuri [137], J. D. Mulligan [75], A. Mulliri [23],

M. G. Munhoz[112], R. H. Munzer[65], H. Murakami[126], S. Murray[116], L. Musa[33], J. Musinsky[61], J. W. Myrcha[138],
B. Naik[125], A. I. Nambrath[19], B. K. Nandi[48], R. Nania[52], E. Nappi[51], A. F. Nassirpour[18], A. Nath[95],
C. Nattrass[124], M. N. Naydenov[37], A. Neagu[20], A. Negru[115], E. Nekrasova[143], L. Nellen[66], R. Nepeivoda[76],
S. Nese[20], G. Neskovic[39], N. Nicassio[51], B. S. Nielsen[84], E. G. Nielsen[84], S. Nikolaev[143], S. Nikulin[143],
V. Nikulin[143], F. Noferini[52], S. Noh[12], P. Nomokonov[144], J. Norman[121], N. Novitzky[88], P. Nowakowski[138],
A. Nyanin[143], J. Nystrand[21], S. Oh[18], A. Ohlson[76], V. A. Okorokov[143], J. Oleniacz[138], A. Onnerstad[119],
C. Oppedisano[57], A. Ortiz Velasquez[66], J. Otwinowski[109], M. Oya[93], K. Oyama[77], Y. Pachmayer[95], S. Padhan[48],
D. Pagano[56,136], G. Paić[66], S. Paisano-Guzmán[45], A. Palasciano[51], S. Panebianco[132], H. Park[127], H. Park[106],
J. E. Parkkila[33], Y. Patley[48], B. Paul[23], M. M. D. M. Paulino[112], H. Pei[6], T. Peitzmann[60], X. Peng[11],
M. Pennisi[25], S. Perciballi[25], D. Peresunko[143], G. M. Perez[7], Y. Pestov[143], V. Petrov[143], M. Petrovici[46],
R. P. Pezzi[67,105], S. Piano[58], M. Pikna[13], P. Pillot[105], O. Pinazza[33,52], L. Pinsky[118], C. Pinto[96], S. Pisano[50],
M. Płoskoń[75], M. Planinic[90], F. Pliquett[65], M. G. Poghosyan[88], B. Polichtchouk[143], S. Politano[30], N. Poljak[90],
A. Pop[46], S. Porteboeuf-Houssais[129], V. Pozdniakov[144,†], I. Y. Pozos[45], K. K. Pradhan[49], S. K. Prasad[4],
S. Prasad[49], R. Preghenella[52], F. Prino[57], C. A. Pruneau[139], I. Pshenichnov[143], M. Puccio[33], S. Pucillo[25],
S. Qiu[85], L. Quaglia[25], S. Ragoni[15], A. Rai[140], A. Rakotozafindrabe[132], L. Ramello[57,135], F. Rami[131],
M. Rasa[27], S. S. Räsänen[44], R. Rath[52], M. P. Rauch[21], I. Ravasenga[33], K. F. Read[88,124], C. Reckziegel[114],
A. R. Redelbach[39], K. Redlich[80,§§], C. A. Reetz[98], H. D. Regules-Medel[45], A. Rehman[21], F. Reidt[33],
H. A. Reme-Ness[35], Z. Rescakova[38], K. Reygers[95], A. Riabov[143], V. Riabov[143], R. Ricci[29], M. Richter[21],
A. A. Riedel[96], W. Riegler[33], A. G. Riffero[25], C. Ripoli[29], C. Ristea[64], M. V. Rodriguez[33],
M. Rodríguez Cahuantzi[45], S. A. Rodríguez Ramírez[45], K. Røed[20], R. Rogalev[143], E. Rogochaya[144],
T. S. Rogoschinski[65], D. Rohr[33], D. Röhrich[21], S. Rojas Torres[36], P. S. Rokita[138], G. Romanenko[26],
F. Ronchetti[50], E. D. Rosas[66], K. Roslon[138], A. Rossi[55], A. Roy[49], S. Roy[48], N. Rubini[26], D. Ruggiano[138],
R. Rui[24], P. G. Russek[2], R. Russo[85], A. Rustamov[82], E. Ryabinkin[143], Y. Ryabov[143], A. Rybicki[109], J. Ryu[17],
W. Rzesa[138], O. A. M. Saarimaki[44], S. Sadhu[32], S. Sadovsky[143], J. Saetre[21], K. Šafařík[36], S. K. Saha[4],
S. Saha[81], B. Sahoo[49], R. Sahoo[49], S. Sahoo[62], D. Sahu[49], P. K. Sahu[62], J. Saini[137], K. Sajdakova[38], S. Sakai[127],
M. P. Salvan[98], S. Sambyal[92], D. Samitz[104], I. Sanna[33,96], T. B. Saramela[112], D. Sarkar[84], P. Sarma[42],
V. Sarritzu[23], V. M. Sarti[96], M. H. P. Sas[33], S. Sawan[81], E. Scapparone[52], J. Schambach[88], H. S. Scheid[65],
C. Schiaua[46], R. Schicker[95], F. Schlepper[95], A. Schmah[98], C. Schmidt[98], H. R. Schmidt[94], M. O. Schmidt[33],
M. Schmidt[94], N. V. Schmidt[88], A. R. Schmier[124], R. Schotter[131], A. Schröter[39], J. Schukraft[33], K. Schweda[98],
G. Scioli[26], E. Scomparin[57], J. E. Seger[15], Y. Sekiguchi[126], D. Sekihata[126], M. Selina[85], I. Selyuzhenkov[98],
S. Senyukov[131], J. J. Seo[95], D. Serebryakov[143], L. Serkin[66], L. Šerkšnytė[96], A. Sevcenco[64], T. J. Shaba[69],
A. Shabetai[105], R. Shahoyan[33], A. Shangaraev[143], B. Sharma[92], D. Sharma[48], H. Sharma[55], M. Sharma[92],
S. Sharma[77], S. Sharma[92], U. Sharma[92], A. Shatat[133], O. Sheibani[118], K. Shigaki[93], M. Shimomura[78], J. Shin[12],
S. Shirinkin[143], Q. Shou[40], Y. Sibiriak[143], S. Siddhanta[53], T. Siemiarczuk[80], T. F. Silva[112], D. Silvermyr[76],
T. Simantathammakul[107], R. Simeonov[37], B. Singh[92], B. Singh[96], K. Singh[49], R. Singh[81], R. Singh[92],
R. Singh[49,98], S. Singh[16], V. K. Singh[137], V. Singhal[137], T. Sinha[101], B. Sitar[13], M. Sitta[57,135], T. B. Skaali[20],
G. Skorodumovs[95], N. Smirnov[140], R. J. M. Snellings[60], E. H. Solheim[20], J. Song[17], C. Sonnabend[33,98],
J. M. Sonneveld[85], F. Soramel[28], A. B. Soto-hernandez[89], R. Spijkers[85], I. Sputowska[109], J. Staa[76], J. Stachel[95],
I. Stan[64], P. J. Steffanic[124], S. F. Stiefelmaier[95], D. Stocco[105], I. Storehaug[20], N. J. Strangmann[65],
P. Stratmann[128], S. Strazzi[26], A. Sturniolo[31,54], C. P. Stylianidis[85], A. A. P. Suaide[112], C. Suire[133], M. Sukhanov[143],
M. Suljic[33], R. Sultanov[143], V. Sumberia[92], S. Sumowidagdo[83], I. Szarka[13], M. Szymkowski[138], S. F. Taghavi[96],
G. Taillepied[98], J. Takahashi[113], G. J. Tambave[81], S. Tang[6], Z. Tang[122], J. D. Tapia Takaki[120], N. Tapus[115],
L. A. Tarasovicova[128], M. G. Tarzila[46], G. F. Tassielli[32], A. Tauro[33], A. Tavira García[133], G. Tejeda Muñoz[45],
A. Telesca[33], L. Terlizzi[25], C. Terrevoli[51], S. Thakur[4], D. Thomas[110], A. Tikhonov[143], N. Tiltmann[33,128],
A. R. Timmins[118], M. Tkacik[108], T. Tkacik[108], A. Toia[65], R. Tokumoto[93], S. Tomassini[26], K. Tomohiro[93],
N. Topilskaya[143], M. Toppi[50], T. Tork[133], V. V. Torres[105], A. G. Torres Ramos[32], A. Trifiró[31,54],
A. S. Triolo[31,33,54], S. Tripathy[52], T. Tripathy[48], V. Trubnikov[3], W. H. Trzaska[119], T. P. Trzcinski[138],
A. Tumkin[143], R. Turrisi[55], T. S. Tveter[20], K. Ullaland[21], B. Ulukutlu[96], A. Uras[130], M. Urioni[136], G. L. Usai[23],
M. Vala[38], N. Valle[56], L. V. R. van Doremalen[60], M. van Leeuwen[85], C. A. van Veen[95], R. J. G. van Weelden[85],

P. Vande Vyvre[33] D. Varga,[47] Z. Varga[47] P. Vargas Torres,[66] M. Vasileiou,[79] A. Vasiliev,[143] O. Vázquez Doce[50] O. Vazquez Rueda[118] V. Vechernin,[143] E. Vercellin,[25] S. Vergara Limón,[45] R. Verma,[48] L. Vermunt,[98] R. Vértesi[47] M. Verweij,[60] L. Vickovic,[34] Z. Vilakazi,[125] O. Villalobos Baillie,[102] A. Villani,[24] A. Vinogradov,[143] T. Virgili[29] M. M. O. Virta[119] V. Vislavicius,[76] A. Vodopyanov[144] B. Volkel[33] M. A. Völkl[95] S. A. Voloshin,[139] G. Volpe[32] B. von Haller[33] I. Vorobyev[33] N. Vozniuk[143] J. Vrláková,[38] J. Wan,[40] C. Wang,[40] D. Wang,[40] Y. Wang[40] Y. Wang[6] A. Wegrzynek[33] F. T. Weiglhofer,[39] S. C. Wenzel[33] J. P. Wessels[128] J. Wiechula,[65] J. Wikne,[20] G. Wilk[80] J. Wilkinson,[98] G. A. Willems[128] B. Windelband[95] M. Winn,[132] J. R. Wright,[110] W. Wu,[40] Y. Wu[122] Z. Xiong,[122] R. Xu[6] A. Yadav,[43] A. K. Yadav,[137] S. Yalcin,[73] Y. Yamaguchi[93] S. Yang,[21] S. Yano[93] E. R. Yeats,[19] Z. Yin[6] I.-K. Yoo,[17] J. H. Yoon,[59] H. Yu,[12] S. Yuan,[21] A. Yuncu,[95] V. Zaccolo,[24] C. Zampolli[33] M. Zang,[6] F. Zanone[95] N. Zardoshti,[33] A. Zarochentsev,[143] P. Závada,[63] N. Zaviyalov,[143] M. Zhalov[143] B. Zhang[6] C. Zhang[132] L. Zhang[40] M. Zhang,[6] S. Zhang[40] X. Zhang[6] Y. Zhang,[122] Z. Zhang[6] M. Zhao,[10] V. Zherebchevskii[143] Y. Zhi,[10] C. Zhong,[40] D. Zhou[6] Y. Zhou,[84] J. Zhu[6,55] Y. Zhu,[6] S. C. Zugravel[57] and N. Zurlo[56,136]

(ALICE Collaboration)

[1]*A.I. Alikhanyan National Science Laboratory (Yerevan Physics Institute) Foundation, Yerevan, Armenia*
[2]*AGH University of Krakow, Cracow, Poland*
[3]*Bogolyubov Institute for Theoretical Physics, National Academy of Sciences of Ukraine, Kiev, Ukraine*
[4]*Bose Institute, Department of Physics and Centre for Astroparticle Physics and Space Science (CAPSS), Kolkata, India*
[5]*California Polytechnic State University, San Luis Obispo, California, USA*
[6]*Central China Normal University, Wuhan, China*
[7]*Centro de Aplicaciones Tecnológicas y Desarrollo Nuclear (CEADEN), Havana, Cuba*
[8]*Centro de Investigación y de Estudios Avanzados (CINVESTAV), Mexico City and Mérida, Mexico*
[9]*Chicago State University, Chicago, Illinois, USA*
[10]*China Institute of Atomic Energy, Beijing, China*
[11]*China University of Geosciences, Wuhan, China*
[12]*Chungbuk National University, Cheongju, Republic of Korea*
[13]*Comenius University Bratislava, Faculty of Mathematics, Physics and Informatics, Bratislava, Slovak Republic*
[14]*COMSATS University Islamabad, Islamabad, Pakistan*
[15]*Creighton University, Omaha, Nebraska, USA*
[16]*Department of Physics, Aligarh Muslim University, Aligarh, India*
[17]*Department of Physics, Pusan National University, Pusan, Republic of Korea*
[18]*Department of Physics, Sejong University, Seoul, Republic of Korea*
[19]*Department of Physics, University of California, Berkeley, California, USA*
[20]*Department of Physics, University of Oslo, Oslo, Norway*
[21]*Department of Physics and Technology, University of Bergen, Bergen, Norway*
[22]*Dipartimento di Fisica, Università di Pavia, Pavia, Italy*
[23]*Dipartimento di Fisica dell'Università and Sezione INFN, Cagliari, Italy*
[24]*Dipartimento di Fisica dell'Università and Sezione INFN, Trieste, Italy*
[25]*Dipartimento di Fisica dell'Università and Sezione INFN, Turin, Italy*
[26]*Dipartimento di Fisica e Astronomia dell'Università and Sezione INFN, Bologna, Italy*
[27]*Dipartimento di Fisica e Astronomia dell'Università and Sezione INFN, Catania, Italy*
[28]*Dipartimento di Fisica e Astronomia dell'Università and Sezione INFN, Padova, Italy*
[29]*Dipartimento di Fisica "E.R. Caianiello" dell'Università and Gruppo Collegato INFN, Salerno, Italy*
[30]*Dipartimento DISAT del Politecnico and Sezione INFN, Turin, Italy*
[31]*Dipartimento di Scienze MIFT, Università di Messina, Messina, Italy*
[32]*Dipartimento Interateneo di Fisica "M. Merlin" and Sezione INFN, Bari, Italy*
[33]*European Organization for Nuclear Research (CERN), Geneva, Switzerland*
[34]*Faculty of Electrical Engineering, Mechanical Engineering and Naval Architecture, University of Split, Split, Croatia*
[35]*Faculty of Engineering and Science, Western Norway University of Applied Sciences, Bergen, Norway*
[36]*Faculty of Nuclear Sciences and Physical Engineering, Czech Technical University in Prague, Prague, Czech Republic*
[37]*Faculty of Physics, Sofia University, Sofia, Bulgaria*

[38]Faculty of Science, P.J. Šafárik University, Košice, Slovak Republic

[39]Frankfurt Institute for Advanced Studies, Johann Wolfgang Goethe-Universität Frankfurt, Frankfurt, Germany

[40]Fudan University, Shanghai, China

[41]Gangneung-Wonju National University, Gangneung, Republic of Korea

[42]Gauhati University, Department of Physics, Guwahati, India

[43]Helmholtz-Institut für Strahlen-und Kernphysik, Rheinische Friedrich-Wilhelms-Universität Bonn, Bonn, Germany

[44]Helsinki Institute of Physics (HIP), Helsinki, Finland

[45]High Energy Physics Group, Universidad Autónoma de Puebla, Puebla, Mexico

[46]Horia Hulubei National Institute of Physics and Nuclear Engineering, Bucharest, Romania

[47]HUN-REN Wigner Research Centre for Physics, Budapest, Hungary

[48]Indian Institute of Technology Bombay (IIT), Mumbai, India

[49]Indian Institute of Technology Indore, Indore, India

[50]INFN, Laboratori Nazionali di Frascati, Frascati, Italy

[51]INFN, Sezione di Bari, Bari, Italy

[52]INFN, Sezione di Bologna, Bologna, Italy

[53]INFN, Sezione di Cagliari, Cagliari, Italy

[54]INFN, Sezione di Catania, Catania, Italy

[55]INFN, Sezione di Padova, Padova, Italy

[56]INFN, Sezione di Pavia, Pavia, Italy

[57]INFN, Sezione di Torino, Turin, Italy

[58]INFN, Sezione di Trieste, Trieste, Italy

[59]Inha University, Incheon, Republic of Korea

[60]Institute for Gravitational and Subatomic Physics (GRASP), Utrecht University/Nikhef, Utrecht, Netherlands

[61]Institute of Experimental Physics, Slovak Academy of Sciences, Košice, Slovak Republic

[62]Institute of Physics, Homi Bhabha National Institute, Bhubaneswar, India

[63]Institute of Physics of the Czech Academy of Sciences, Prague, Czech Republic

[64]Institute of Space Science (ISS), Bucharest, Romania

[65]Institut für Kernphysik, Johann Wolfgang Goethe-Universität Frankfurt, Frankfurt, Germany

[66]Instituto de Ciencias Nucleares, Universidad Nacional Autónoma de México, Mexico City, Mexico

[67]Instituto de Física, Universidade Federal do Rio Grande do Sul (UFRGS), Porto Alegre, Brazil

[68]Instituto de Física, Universidad Nacional Autónoma de México, Mexico City, Mexico

[69]iThemba LABS, National Research Foundation, Somerset West, South Africa

[70]Jeonbuk National University, Jeonju, Republic of Korea

[71]Johann-Wolfgang-Goethe Universität Frankfurt Institut für Informatik, Fachbereich Informatik und Mathematik, Frankfurt, Germany

[72]Korea Institute of Science and Technology Information, Daejeon, Republic of Korea

[73]KTO Karatay University, Konya, Turkey

[74]Laboratoire de Physique Subatomique et de Cosmologie, Université Grenoble-Alpes, CNRS-IN2P3, Grenoble, France

[75]Lawrence Berkeley National Laboratory, Berkeley, California, USA

[76]Lund University Department of Physics, Division of Particle Physics, Lund, Sweden

[77]Nagasaki Institute of Applied Science, Nagasaki, Japan

[78]Nara Women's University (NWU), Nara, Japan

[79]National and Kapodistrian University of Athens, School of Science, Department of Physics, Athens, Greece

[80]National Centre for Nuclear Research, Warsaw, Poland

[81]National Institute of Science Education and Research, Homi Bhabha National Institute, Jatni, India

[82]National Nuclear Research Center, Baku, Azerbaijan

[83]National Research and Innovation Agency—BRIN, Jakarta, Indonesia

[84]Niels Bohr Institute, University of Copenhagen, Copenhagen, Denmark

[85]Nikhef, National institute for subatomic physics, Amsterdam, Netherlands

[86]Nuclear Physics Group, STFC Daresbury Laboratory, Daresbury, United Kingdom

[87]Nuclear Physics Institute of the Czech Academy of Sciences, Husinec-Řež, Czech Republic

[88]Oak Ridge National Laboratory, Oak Ridge, Tennessee, USA

[89]Ohio State University, Columbus, Ohio, USA

[90]Physics Department, Faculty of Science, University of Zagreb, Zagreb, Croatia

[91]Physics Department, Panjab University, Chandigarh, India

[92]Physics Department, University of Jammu, Jammu, India

[93]Physics Program and International Institute for Sustainability with Knotted Chiral Meta Matter (SKCM2), Hiroshima University, Hiroshima, Japan

[94]Physikalisches Institut, Eberhard-Karls-Universität Tübingen, Tübingen, Germany

[95]Physikalisches Institut, Ruprecht-Karls-Universität Heidelberg, Heidelberg, Germany

[96]Physik Department, Technische Universität München, Munich, Germany

[97]Politecnico di Bari and Sezione INFN, Bari, Italy

[98]Research Division and ExtreMe Matter Institute EMMI, GSI Helmholtzzentrum für Schwerionenforschung GmbH, Darmstadt, Germany

[99]RIKEN iTHEMS, Wako, Japan

[100]Saga University, Saga, Japan

[101]Saha Institute of Nuclear Physics, Homi Bhabha National Institute, Kolkata, India

[102]School of Physics and Astronomy, University of Birmingham, Birmingham, United Kingdom

[103]Sección Física, Departamento de Ciencias, Pontificia Universidad Católica del Perú, Lima, Peru

[104]Stefan Meyer Institut für Subatomare Physik (SMI), Vienna, Austria

[105]SUBATECH, IMT Atlantique, Nantes Université, CNRS-IN2P3, Nantes, France

[106]Sungkyunkwan University, Suwon City, Republic of Korea

[107]Suranaree University of Technology, Nakhon Ratchasima, Thailand

[108]Technical University of Košice, Košice, Slovak Republic

[109]The Henryk Niewodniczanski Institute of Nuclear Physics, Polish Academy of Sciences, Cracow, Poland

[110]The University of Texas at Austin, Austin, Texas, USA

[111]Universidad Autónoma de Sinaloa, Culiacán, Mexico

[112]Universidade de Sao Paulo (USP), Sao Paulo, Brazil

[113]Universidade Estadual de Campinas (UNICAMP), Campinas, Brazil

[114]Universidade Federal do ABC, Santo Andre, Brazil

[115]Universitatea Nationala de Stiinta si Tehnologie Politehnica Bucuresti, Bucharest, Romania

[116]University of Cape Town, Cape Town, South Africa

[117]University of Derby, Derby, United Kingdom

[118]University of Houston, Houston, Texas, USA

[119]University of Jyväskylä, Jyväskylä, Finland

[120]University of Kansas, Lawrence, Kansas, USA

[121]University of Liverpool, Liverpool, United Kingdom

[122]University of Science and Technology of China, Hefei, China

[123]University of South-Eastern Norway, Kongsberg, Norway

[124]University of Tennessee, Knoxville, Tennessee, USA

[125]University of the Witwatersrand, Johannesburg, South Africa

[126]University of Tokyo, Tokyo, Japan

[127]University of Tsukuba, Tsukuba, Japan

[128]Universität Münster, Institut für Kernphysik, Münster, Germany

[129]Université Clermont Auvergne, CNRS/IN2P3, LPC, Clermont-Ferrand, France

[130]Université de Lyon, CNRS/IN2P3, Institut de Physique des 2 Infinis de Lyon, Lyon, France

[131]Université de Strasbourg, CNRS, IPHC UMR 7178, F-67000 Strasbourg, France, Strasbourg, France

[132]Université Paris-Saclay, Centre d'Etudes de Saclay (CEA), IRFU, Départment de Physique Nucléaire (DPhN), Saclay, France

[133]Université Paris-Saclay, CNRS/IN2P3, IJCLab, Orsay, France

[134]Università degli Studi di Foggia, Foggia, Italy

[135]Università del Piemonte Orientale, Vercelli, Italy

[136]Università di Brescia, Brescia, Italy

[137]Variable Energy Cyclotron Centre, Homi Bhabha National Institute, Kolkata, India

[138]Warsaw University of Technology, Warsaw, Poland

[139]Wayne State University, Detroit, Michigan, USA

[140]Yale University, New Haven, Connecticut, USA

[141]Yonsei University, Seoul, Republic of Korea

[142]Zentrum für Technologie und Transfer (ZTT), Worms, Germany

[143]Affiliated with an institute covered by a cooperation agreement with CERN

[144]Affiliated with an international laboratory covered by a cooperation agreement with CERN

[†]Deceased.

[‡]Also at Max-Planck-Institut fur Physik, Munich, Germany.

[§]Also at Italian National Agency for New Technologies, Energy and Sustainable Economic Development (ENEA), Bologna, Italy.

[||]Also at Dipartimento DET del Politecnico di Torino, Turin, Italy.
[¶]Also at Helmholtz Institut für Strahlen- und Kernphysik and Bethe Center for Theoretical Physics, Universität Bonn, Bonn, Germany.
[**]Also at Yildiz Technical University, Istanbul, Türkiye.
[††]Also at An institution covered by a cooperation agreement with CERN.
[‡‡]Also at Department of Applied Physics, Aligarh Muslim University, Aligarh, India.
[§§]Also at Institute of Theoretical Physics, University of Wroclaw, Poland.